Structure and mechanism of acetylation by the N-terminal dual enzyme NatA/Naa50 complex

Sunbin Deng[1,2], Robert S. Magin[3], Xuepeng Wei[2,4], Buyan Pan[1], E. James Petersson[1,4], Ronen Marmorstein[1,2,4,*]

[1]Department of Chemistry, University of Pennsylvania, 231 South 34th Street, Philadelphia, PA 19104, USA

[2]Abramson Family Cancer Research Institute, Perelman School of Medicine, University of Pennsylvania, Philadelphia, PA 19104, USA

3Current Address: Department of Cancer Biology, Dana-Farber Cancer Institute, Boston, MA 02215, USA

[4] Department of Biochemistry and Biophysics, Abramson Family Cancer Research Institute, Perelman School of Medicine, University of Pennsylvania, 421 Curie Boulevard, Philadelphia, PA 19104, USA

Running Title: Structure/Function of dual enzyme NatA/Naa50 complex

Lead Contact: To whom correspondence should be addressed: Ronen Marmorstein, Department of Biochemistry & Biophysics, Abramson Family Cancer Research Institute, Perelman School of Medicine at the University of Pennsylvania, 421 Curie Blvd., Philadelphia, PA 19104, USA, Tel.: (215) 898-7740; Fax: (215) 746-5511; email: marmor@upenn.edu

Keywords: N-terminal acetylation; X-ray crystallography; protein complex; NatA; Naa50; NatE

SUMMARY

NatA co-translationally acetylates the N-termini of over 40% of eukaryotic proteins and can associate with another catalytic subunit, Naa50, to form a ternary NatA/Naa50 dual enzyme complex (also called NatE). The molecular basis of association between Naa50 and NatA and the mechanism for how their association affects their catalytic activities in yeast and human are poorly understood. Here we determined the X-ray crystal structure of yeast NatA/Naa50 as a scaffold to understand coregulation of NatA/Naa50 activity in both yeast and human. We find that Naa50 makes evolutionarily conserved contacts to both the Naa10 and Naa15 subunits of NatA. These interactions promote catalytic crosstalk within the human complex, but do so to a lesser extent in the yeast complex, where Naa50 activity is compromised. These studies have implications for understanding the role of the NatA/Naa50 complex in modulating the majority of the N-terminal acetylome in diverse species.

INTRODUCTION

The majority of nascent peptides biosynthesized by the eukaryote cytosolic ribosome undergo several N-terminal co-translational modifications before they become fully functional and mature proteins. Along with initial methionine cleavage by methionine aminopeptidase (iMAP) and N-terminal myristoylation, N-terminal acetylation (Nt-acetylation), which transfers an acetyl moiety from acetyl-CoA to the N-terminal amino group of proteins, is an irreversible, highly conserved and abundant modification (Giglione et al., 2015). About 50-70% of *S. cerevisiae* proteins, 70%-75% of *A. thaliana* proteins, and 70-90% of *H. sapiens* proteins are subject to Nt-acetylation by a family of N-terminal acetyl transferases (NATs) (Starheim et al., 2012). Nt-acetylation is generally considered to be a co-translational process, with most NATs making direct interactions with both nascent peptide and the ribosome

(Gautschi et al., 2003, Polevoda et al., 2008, Magin et al., 2017, Knorr et al., 2018).

Numerous studies have demonstrated that Nt-acetylation can affect diverse protein and cellular activities including gene regulation, apoptosis, protein folding, protein degradation, protein complex formation and subcellular localization (Aksnes et al., 2016, Holmes et al., 2014, Scott et al., 2011, Shemorry et al., Behnia et al., 2004, Yang et al., 2013, Dikiy and Eliezer, 2014, Hwang et al., 2010, Schiza et al., 2013, Starheim et al., 2009, Arnesen et al., 2006b, Setty et al., 2004, Pavlou and Kirmizis, 2016). Knockout of NATs frequently results in severe cellular defects including slow growth and reduced mating efficiency in yeast (Polevoda and Sherman, 2003). In higher eukaryotes, misregulation of N-terminal acetylation can lead to numerous developmental disorders and cancers (Kalvik and Arnesen, 2012, Myklebust et al., 2015, Lee et al., 2010, Yu et al., 2009, Arnesen et al., 2006a, Ametzazurra et al., 2008, Starheim et al., 2008, Starheim et al., 2009, Fluge et al., 2002, Hua et al., 2011). For example, the NatA catalytic subunit, Naa10, plays important roles in mammalian cells including cellular hypoxia, bone formation and DNA damage (Dorfel and Lyon, 2015, Jeong et al., 2002, Yoon et al., 2014, Yi et al., 2007). Mutation in human Naa10 causes the genetic disorder Ogden syndrome (Rope et al., 2011).

Several NATs, including NatA, NatB, NatC, NatD, NatE, and NatF are conserved across eukaryotes (Aksnes et al., 2016) (Aksnes et al., 2015, Aksnes et al., 2017, Stove et al., 2016). NatG is resident in chloroplasts of plant cells (Dinh et al., 2015), and the recently identified NatH/Naa80 exists only in animals to acetylate a subset of processed actins (Drazic et al., 2018). The presence of NatF, NatG, and NatH indicates that this modification can also occur post-translationally. NATs can acetylate the N-termini either when the initiator methionine (iMet) is cleaved or retained, mostly depending on the

identity of the first two amino acids of the nascent peptide (Aksnes et al., 2016), which further enriches the complexity of the eukaryote proteome. Both NatA and NatD complete the process after iMet is cleaved. NatA shows specificity toward the N-termini of exposed A-, S-, T-, V-, C-, and sometimes G-, while NatD can only acetylate the N-terminal serine of histones H2A and H4 (Magin et al., 2015, Gottlieb and Marmorstein, 2018, Liszczak et al., 2013, Arnesen et al., 2009a, Song et al., 2003). Other NATs like NatB, NatC, NatE, and NatF modify peptides with the iMet retained. NatB prefers the Met-Asx/Glx type N-termini (MD-, ME-, MN-, and MQ-starting) , whereas NatC, NatE, and NatF have some substrate overlap, and they acetylate peptides with “hydrophobic/amphipathic” residues like L, I, F, Y, K directly following iMet (Liszczak et al., 2011, Stove et al., 2016, Van Damme et al., 2016, Tercero et al., 1993, Evjenth et al., 2009, Van Damme et al., 2011b). NatA, B and C are the three major contributors to the Nt-acetylome, as they cover about 80% of all NAT substrates (Aksnes et al., 2016). Notably, NatA, B and C contain at least one auxiliary subunit to couple with the catalytic subunit for enzymatic activity towards cognate substrates and anchoring of the catalytic subunit to the ribosome, while NatD, F, G, H are each composed of only one single catalytic subunit. NatE is composed to two catalytic and one auxiliary subunit.

NatA is comprised of the catalytic subunit Naa10 and the auxiliary subunit Naa15 (Liszczak et al., 2013, Gottlieb and Marmorstein, 2018). Naa10 can also exist independently of Naa15, exhibiting altered substrate specificity and might also be involved in transcriptional activity inside the nucleus (Arnesen et al., 2005, Van Damme et al., 2011a). Alternatively, NatA can also form a complex with another catalytic subunit Naa50 to form a ternary NatA/Naa50 complex (also called NatE) (Gautschi et al., 2003), and NatA from some eukaryotic species including *Chaetomium thermophilum* and human exhibit tight binding affinity with a regulatory protein called HYPK (Gottlieb and

Marmorstein, 2018, Weyer et al., 2017, Arnesen et al., 2010). Deletion of Naa50 in yeast shows no phenotype (Gautschi et al., 2003), while Naa50 knockout can affect sister chromatid cohesion in higher organisms like *Drosophila* and human (Hou et al., 2007, Chu et al., 2011, Ribeiro et al., 2016, Williams et al., 2003). Endogenous pulldown of NatA/Naa50 complexes from human cells indicates that over 80% of Naa50 is not associated with NatA *in vivo* (Hou et al., 2007), whereas the remaining ~20% forms a stable and stoichiometric complex. Furthermore, another recent study demonstrates that loss of Naa50 in *Drosophila* leads to a decrease of NatA *in vivo* acetylation activity (Rathore et al., 2016). A recent cryo-EM structure of a yeast NatA/Naa50-ribosome complex with an 8 Å NatA local resolution reveals that both Naa50 and the Naa15 regulatory subunit of NatA contribute to ribosome interaction, with the Naa10 active site about 50 Å from the ribosome exit tunnel, and the Naa50 active site about 2-times that distance (Knorr et al., 2018). The underlying molecular basis for the potential functional coupling and interplay between the catalytic subunits of the NatA/Naa50 complex is still poorly understood.

To understand the molecular basis for NatA/Naa50 co-regulation of N-terminal protein acetylation across species, we determined the X-ray crystal structure of a yeast NatA/Naa50 complex and used it as a scaffold to understand coregulation of NatA/Naa50 activity in yeast and human. We find that NatA/Naa50 forms a stable complex in yeast and human through conserved interactions: Naa50 makes contacts to both the Naa10 and Naa15 subunits of NatA. We demonstrate that NatA-Naa50 interactions can significantly promote the catalytic activities of the two catalytic subunits within the human complex relative to NatA or Naa50 alone. In contrast, in the yeast complex, Naa50 modestly increases the activity of NatA, and Naa50 is defective in catalytic activity, likely through compromised peptide binding. These studies have

implications for understanding the role of the NatA/Naa50 complex in modulating the majority of the N-terminal acetylome in diverse species.

RESULTS

NatA and Naa50 form stable complexes in yeast and human

We used recombinant proteins to characterize the interaction between Naa50 and NatA from human (h) and *S. pombe* (*Sp*) *in vitro*. Recombinant SpNatA, SpNaa50, and human Naa50 were overexpressed and purified from *E. coli*, while hNatA was prepared from baculovirus-infected Sf9 insect cells. Consistent with previous data reporting a direct interaction between NatA and Naa50 (Gautschi et al., 2003, Hou et al., 2007), we found that N-terminal GST-tagged Naa50 can pull-down NatA. We also found that human and *S. pombe* NatA and Naa50 co-migrate by size-exclusion chromatography to form stochiometric complexes under near native salt concentration (200 mM NaCl) **(Figure 1A)**. Interestingly, *Sp*Naa50 maintained the ability to co-migrate with *Sp*NatA in sizing buffer with NaCl concentration as high as 1 M **(Figure 1A)**, suggesting that this interaction in *S. pombe* is robust and not dominated by electrostatic interactions, while hNatA and hNaa50 failed to form a stochiometric complex in the high salt buffer **(Figure 1A)** suggesting some divergence of the NatA-Naa50 interaction between the yeast and human complexes. In addition, we observed that SpNaa50 displays similar comigration with ScNatA under both native and high NaCl concentrations (**Figure 1A**), strongly indicating that the NatA-Naa50 interaction within yeast is highly conserved.

To more quantitatively asses the interaction between NatA and Naa50, we carried out a Fluorescence Polarization (FP) assay, using Naa50 labeled with Fluorescein-5-Maleimide via exposed surface cysteines. We observed that Naa50 tightly binds to NatA in both the *S. pombe* and human systems with K_d values of 17 ± 3.4 nM and 29 ± 5.6 nM, respectively (**Figure 1B**). These data,

together with the high degree of sequence conservation of the interaction interfaces between Naa50 and NatA in the two species (**Figures S1-S3**), suggest that Naa50 and NatA from yeast and human are very likely to have similar association mechanisms. However, we found that GST-hNaa50 failed to pull down *Sp*NatA, and that hNaa50 and *Sp*NatA could not form a stoichiometric complex in size-exclusion chromatography (data not shown), indicating that the details of the hNatA/Naa50 interaction have diverged over evolutionary time. This was further validated using differential scanning fluorimetry experiments, where we found that the addition of SpNaa50 to *Sp*NatA and hNaa50 to hNatA had thermal melting temperature increases of 37.8 °C to 40.4 °C and 44 °C to 46.6 °C, respectively; while the addition of hNaa50 to SpNatA had a thermal melting temperature of 37.5 °C, very close to *Sp*NatA alone (**Figure 1C**). Notably, SpNaa50 significantly extended the melting temperature of ScNatA by 7.4°C, further confirming the existence of a conserved robust interaction across these two yeast species **(Figure 1C)**.

Crystal structure of the ternary NatA/Naa50 complex shows that Naa50 contacts both subunits of NatA

To reveal the molecular basis for the association and regulation mechanism of the NatA/Naa50 complex, we determined its crystal structure. We were unable to obtain crystals of the human complex, and crystals of the *S. pombe* complex diffracted X-rays poorly. However, we found that full-length ScNaa15 (residues 1–854) from *S. cerevisiae* (*Sc*) with a C-terminal truncation of ScNaa10 (1–226 out of 238 total residues) and full-length ScNaa50 (residues 1–176) produced crystals with good diffraction quality, in the presence of inositol hexaphosphate (IP6) and bi-substrate analogs for both Naa50 and Naa10. The crystals formed in the $P2_12_12_1$ space group with one ternary complex in the asymmetric unit. The diffraction data set was collected to 2.7 Å resolution, and the structure was determined by molecular replacement with an unpublished *Sc*NatE complex (Protein Data Bank code: 4XNH) as an initial

search model. The final structure was refined to R_{work} and R_{free} values of 22.21% and 25.03%, respectively. Refinement statistics can be found in **Table 1**.

Not surprisingly, the *Sc*Naa15 auxiliary subunit of NatA displays a high degree of structure conservation with *Sp*Naa15 and hNaa15, with root-mean square deviation of 1.409 Å (over 577 common C_α atoms) and 1.537 Å (over 640 common C_α atoms), respectively. Shaped like a horseshoe, ScNaa15 is comprised of 15 TPR motifs, which often mediate protein-protein interactions. The electron density for the first two alpha helices (N terminal 1-53 residues) is poorly resolved and not built in our model **(Figure S1)**. This auxiliary subunit, consisting of a total 42 α-helices, serves as the binding scaffold for both catalytic subunits. *Sc*Naa10 is completely wrapped by the Naa15 helices (from α11 to α30, encompassing residues Lys198- Gly595) with extensive interactions, with an overall contact surface area of 3555.5 $Å^2$ (**Figure 2A**). The longest alpha helix is α29, expanding to be as long as 70 Å across almost the entire length of the protein. This extremely long helix bridges the overall ring-like tertiary structure of Naa15 and locks Naa10 into the well-formed cradle made by the surrounding helices. Naa50 sits adjacent to Naa10 and interacts mostly with several Naa15 helices (α21, α22, α23, α24, encompassing residues Pro380-Asp448), and more modestly with the β2-β3 loop of Naa10, with an overall contact surface area of only 632.3 $Å^2$ (**Figure 2B**).

The significantly less contact surface between Naa50 and Naa15, relative to between Naa10 and Naa15, is probably one reason that Naa50 in this ternary complex displays surprising flexibility, as indicated by its high average B factor (87.6 $Å^2$) compared to Naa10 (48.9 $Å^2$) and Naa15 (56.2 $Å^2$). Several Naa50 residues away from the Naa50-Naa15 interface have poor side chain density and are therefore modeled as alanine residues and some parts of α helices

and β strands are built as loops. Interestingly, the NatA bisubstrate analog used in the cocrystallization could not be resolved due to its poor electron density and was therefore omitted from the model, while only the CoA portion of the Naa50 bisubstrate inhibitor was well resolved and are therefore included in the model.

Previous studies have revealed that human NatA contains a bound IP6 molecule that bridges interactions between helices α19, α24, α25 of hNaa15 and the β2-loop-β3 of hNaa10 (Gottlieb and Marmorstein, 2018). To identify whether a similar IP6 binding pocket exists in *Sc*NatA, IP6 was added to the crystallization of the ternary *Sc*NatA/Naa50 complex. Clear electron density for IP6 was visible between Naa10 and Naa15 (**Figure S4**), in almost the same position identified in the corresponding human NatA complex (data not shown). Extensive electropositive and hydrogen-bond interactions contribute to this interaction including K80, Y85, and K91 from Naa10, and K429, K457, R464, R426, H430 and Y461 from Naa15 **(Figure 2C**). All these residues in Naa15 are conserved from yeast to human **(Figure S1**), which suggests that this binding mode is structurally conserved. We validated the conserved intimate binding of IP6 by also showing its robust binding to *Sp*NatA using isothermal titration calorimetry (ITC), measuring a dissociation constant of ~130 nM, with a 1:1 stoichiometry **(Figure 2D)**.

Hydrophobic interactions dominate the ScNatA-ScNaa50 binding interface

The NatA/Naa50 structure reveals that Naa15 is the primary docking site for Naa50. The contact interface is mediated primarily by the Naa50 β2-β3 and β4-α2 loops with the Naa15 α22-α23 loop. These regions form a network of hydrophobic interactions mediated by several non-polar residues, including Met18, Leu22, Tyr65, Pro70, and Val71 from Naa50 and Leu447, Val418, Thr416, Leu417 from Naa15 **(Figure 3A**). A few H-bonds are observed: the

Naa15 Thr414 sidechain bridges and interaction with the side chain of Naa50 Tyr102 and Naa15 His413, and the Naa15 Thr416 sidechain interacts with the backbone carbonyl group of Naa50 Pro70 **(Figure 3A**). The largely hydrophobic nature of the interface is consistent with our biochemical observation that the *Sp*NatA and Naa50 interaction can be maintained under high salt. Importantly, we found that the TPTLXE (where X represents either V or I) motif in the Naa15 α20-α21 loop is highly conserved in both yeast and human, thus suggesting that yeast and human share a similar NatA-Naa50 binding mode **(Figure S1**).

Unlike Naa10, which is surrounded on all sides by interactions with Naa15 helical segments, thereby locking Naa10 in place, contacts between Naa50 and Naa10 are more modest and mediated by the α3-β4 loop of Naa10. Specifically, contact between Naa10 and Naa50 involves several basic residues within the α3-β4 loop of Naa10 (Arg122, Arg125 and Arg126) and Glu68 within the β2-β3 of Naa50, which make a network of electrostatic interactions **(Figure 3B)**. The distance of Glu68 to Arg122, Arg125 and Arg126 is 2.3 Å,3.8 Å, and 6.2 Å, respectively. The relative paucity of Naa50-NatA interactions likely allows Naa50 to be conformationally flexible to allow it to impose regulatory effects on Naa10 activity. Supporting this notion is the fact that Naa10 Arg125 is the first conserved residue of the acetyl-CoA binding motif Q/RxxGxG/A **(Figure S2)**.

The NatA/Naa50 complex promotes catalytic crosstalk

Since deletion of ScNaa50 shows no phenotype (Gautschi et al., 2003), while Naa50 knockout in higher organisms has been shown to perturb sister chromatid cohesion (Hou et al., 2007, Chu et al., 2011, Ribeiro et al., 2016) and NatA acetylation activity *in vivo* (Rathore et al., 2016), we hypothesized that there might be fundamental functional differences in the catalytic properties of Naa50 within the NatA/Naa50 complexes in yeast and human.

To test this hypothesis, we took advantage of the fact that NatA and Naa50 have distinct substrate preferences. Canonical NatA substrates include peptides with the first four amino acids of SASE (Arnesen et al., 2009b, Liszczak et al., 2013) (hereinafter called “SASE peptide”) and Naa50 substrates include peptides with the first four amino acids MLGP (Liszczak et al., 2011, Evjenth et al., 2009) (hereinafter called “MLGP peptide”). These peptides were used because of their high specificity by their cognate NATs. For our kinetic analysis, we ignored any background activity contribution of NatA toward MLGP peptide and Naa50 toward SASE peptide, based on our data that NatA has negligible activity towards an MLGP peptide (**Figure 7**) and previously published data showing that Naa50 has negligible activity towards non-methionine containing N-termini (Evjenth et al., 2009).

We found that hNaa50, either alone or in complex with hNatA, harbored robust *in vitro* acetylation activity toward the Naa50 cognate peptide, MLGP (**Figure 4A**). Unlike hNaa50, we found that both SpNaa50 alone or with SpNatA, and ScNaa50 alone or with ScNatA, were enzymatically inactive toward the MLGP peptide (**Figure 4A**), consistent with the reported lack of *in vivo* phenotype of ScNaa50 deletion (Gautschi et al., 2003). Notably, we found that that hNaa50 activity was significantly promoted within the ternary hNatA/Naa50 complex **(Figure 4B)**. Indeed, kinetic analysis as a function of peptide substrate demonstrated that hNaa50 harbored a 14-fold decrease in K_m value and 11-fold increase of catalytic efficiency when bound to hNatA **(Figure 4B, Table 2)**. The dramatic change in K_m value suggested that either hNaa15 or hNaa10 can affect hsNaa50 activity by increasing its substrate binding affinity.

We also investigated the effect of Naa50 binding on hNatA activity towards its cognate SASE peptide in both the yeast and human systems. We observed that hNatA showed about a 2.29-fold decrease of K_m value and 1.75-fold

decrease of V_{max} when it bound to hNaa50 **(Figure 4C, Table 2)**. Similarly, we found that SpNatA showed about a 2.45-fold decrease of K_m value and 1.60-fold decrease of V_{max} when bound to *Sp*Naa50 **(Figure 4D, Table 2)**. Overall, *Sp*NatA and hNatA showed comparably significant but modest increases in catalytic efficiencies of 1.53-fold and 1.31-fold, respectively. It is noteworthy that both the Naa10 catalytic subunit of the NatA complex and hNaa50 display a lower K_m for peptide when in the ternary complex, while *Sp*Naa10 also displays a lower K_m in the yeast complex. Taken together, we conclude that the acetylation activities of both catalytic subunits- Naa10 and Naa50 are promoted in this ternary human NatA/Naa50 complex and Naa10 activity is more modestly promoted in the *S. pombe* complex.

Narrow substrate binding sites likely contribute to the catalytic inactivity of yeast Naa50s

Since we were unable to observe catalytic activity for *Sp*Naa50 and ScNaa50, we were surprised to observe electron density in the *Sc*Naa50 active site that could be used to model the acetyl-CoA portion of the acetyl-CoA-MLGP bisubstrate inhibitor that was used in the cocrystallization. Moreover, sequence alignment of Naa50 in human and yeast reveals that *Sp*Naa50 and *Sc*Naa50 do not contain an optimal Q/RxxGxG/A consensus acetyl-CoA binding motif, where in both *Sp*Naa50 and *Sc*Naa50 the first glycine residue is replaced with a serine residue **(Figure S3**). Using ITC, we were able to detect acetyl-CoA binding to hNaa50 **(Figure 5A**) but not to *Sp*Naa50 (**Figure 5B**). We also observed that the *Sp*NatA/Naa50 complex bound acetyl-CoA about 4.5-fold more strongly than *Sp*NatA alone **(Figures 5C and 5D**). Given that SpNaa50 alone binding is not detected in ITC, we propose that the 4.5-fold increase in acetyl-CoA binding affinity for *Sp*NatA/Naa50 relative to *Sp*NatA alone suggests that *Sp*Naa50 binding to *Sp*NatA facilitates acetyl-CoA binding activity to *Sp*NatA. This is consistent with our structural observation that *Sc*Naa50 sits closely to the Q/RxxGxG/A acetyl-CoA binding motif of

*Sc*Naa10, and thereby able to modulate the acetyl-CoA binding activity of *Sc*NatA. Surprisingly, binding signal was detected by ITC between GST-ScNaa50 and acetyl-CoA **(Figure 5 E)**, but not the free GST or GST-*Sp*Naa50 controls **(Figure 5F and 5G)**. This result suggests that the lack of acetyltransferase activity of *Sc*Naa50 is unlikely due to a defect in acetyl CoA binding.

Consistent with the catalytic inactivity of *Sp*Naa50 and ScNaa50, we found that the α1-α2 and β6-β7 loops of ScNaa50 that typically flank the peptide substrate, form a much narrower groove compared to hNaa50 for peptide binding, with the most intimate distance between the loops of less than 2.8 Å **(Figure 5H)**. In addition, both *Sp*Naa50 and *Sc*Naa50 lack the characteristic YY motif found in the β6-β7 loop which is important for substrate binding in all NATs except for Naa40 and Naa80 (**Figure S3**)(Liszczak et al., 2013, Liszczak et al., 2011, Magin et al., 2015, Goris et al., 2018, Hong et al., 2017, Aksnes et al., 2015). Taken together, it appears that the acetyl-CoA and N-terminal peptide substrate binding sites of *Sp*Naa50 are not properly configured for catalytic activity, while *Sc*Naa50 binds acetyl-CoA but likely does not bind peptide substrate.

NatA-Naa50 from yeast and human make conserved interactions

To evaluate the degree of evolutionary conservation of the NatA-Naa50 interface, we first used the *Sc*NatA/Naa50 complex as a scaffold to carry out mutagenesis and binding studies of the yeast NatA/Naa50 complex, using *S. pombe* for mutagenesis for consistency with the earlier biochemical studies in *S. pombe*. Superimposition of the *Sc*NatA/Naa50 and *Sp*NatA structures highlighted a few potential key *S. pombe* candidate residues for interaction, including *Sp*Naa10 R117, *Sp*Naa15 T412, and *Sp*Naa50 Y49 and V53 (**Figures 3 and S1-S3**). Using pull-down assays, we demonstrated that *Sp*Naa10-R117E had an insignificant effect on *Sp*NatA binding, while

*Sp*Naa50-V53K and -Y49A displayed some decrease in *Sp*NatA binding (**Figure 6A, left**). As expected, the double mutation, *Sp*Naa50- Y49A/V53K was significantly defective in *Sp*NatA and *Sc*NatA binding (**Figure 6A**). As these two residues are conserved from yeast to human, it was not surprising that the double mutation of hNaa50-Y50A/I54K displayed similar defects in hNatA binding. The *Sc*NatA/Naa50 crystal structure reveals that *Sc*NatA-T412 sits roughly in the middle position of the conserved Naa15 TPTLXE motif and is located in the center of the binding interface within Naa15 and Naa50 **(Figure 3A**). Interestingly, we found that a single *Sp*Naa15-T412 mutation to either tyrosine or lysine completely disrupted complex formation with *Sp*Naa50 (**Figure 6A**). As expected, sequence alignment demonstrates that *Sp*Naa15-T412 is well conserved in both human and yeast **(Figure S1**). We further observed that both *Sc*Naa15-T416Y and hNaa15-T406Y (hereinafter referred to as TY mutants) lost their ability to association with Naa50 in pull down assays (**Figure 6A)**. Consistent with the pull-down results (**Figure 6A**), the Naa15 TY mutant from *S. pombe*, *S. cerevisiae* and human did not co-migrate with Naa50 by size-exclusion chromatography (**Figure 6B**). For further studies, we focused on *Sp*NatA T412Y and the conserved hNatA T406Y and characterized their roles in NatA-Naa50 association. While the addition of Naa50 to NatA showed robust binding using a FP assay (**Figure 1A**) and increased thermal melting temperature of NatA by about 2.5 °C using DSF assay (**Figure 1B**), addition of Naa50 to the NatA TY mutants did not show detectable binding (**Figure 7A**) or increase in NatA TY mutant thermal melting temperature (**Figure 7B**). We further tested the effect of the NatA TY mutants on NatA acetylation activity and found that they maintained acetylation activity towards cognate substrates although the hNatA TY mutant showed an apparent increase in acetylation activity relative to WT (**Figure 7C**). The reason for this is unclear. Taken together, the Naa15 TY mutants can disrupt the association between NatA and Naa50 in yeast and human.

These studies highlight the important roles of this conserve threonine residue in the association between Naa50 and NatA.

DISCUSSION

While the molecular basis for acetylation activity by either NatA or Naa50 independently has been previously described, the underlying molecular mechanism of how these enzymes work in complex was poorly understood before this study. Although similar to an unpublished structure of *Sc*NatE that has been deposited in the PDB (4XNH), our reported crystal structure of the *Sc*NatA/Naa50 complex in combination with related biochemical data provides a peer reviewed and comprehensive analysis of the structure and mechanism of acetylation by the N-terminal dual enzyme NatA/Naa50 complex across evolution. Overall, the Naa50 electron density is poorly resolved relative to NatA, which suggested that its association with NatA is likely dynamic. Indeed, the major contact region between Naa50 and Naa15 is mediated by loop-loop interactions, unlike the extensive interactions made between Naa10 and Naa15 within the NatA complex. We also found that *Sc*Naa50 makes direct electrostatic interactions with Naa10, providing a path of contact for Naa10 and Naa50 to influence each other's catalytic functions.

Because of their conserved association motif, the hNaa50 docking site on hNaa15 could be identified, and was further supported by mutational analysis. We propose that the proper distance between Naa10 and Naa50 that is required for cognate acetylation of N-terminal protein substrates by the respective NATs, coupled to the less rigid positioning of Naa50, relative to Naa10, may allow Naa50 to adopt multiple conformations within the NatE complex to facilitate both Naa50 and Naa10 cognate substrate binding. Indeed, we found that hNaa50 and hNatA displayed significant enhancement in substrate affinity and catalytic efficiency in the context of the complex, although such enhancement was not observed in the yeast complex, where

we found that Naa50 is catalytically defective. This is consistent with our structural data showing that unlike Naa10, Naa50 harbors a narrow substrate binding site that is incompatible with N-terminal protein substrate binding. However, we cannot exclude the possibility that yeast Naa50 is enzymatically active against another substrate. Regardless, our findings suggest some evolutionary divergence between yeast and human NatE complexes. Nonetheless, we also found that SpNaa50 does not bind human NatA and vice versa, yet from conservation analysis there is no obvious reason why this should be the case. There may be subtle differences in the yeast and human systems that have co evolved, perhaps to reflect the regulatory role of the HYPK protein in the human but not *S. pombe* and *S. cerevisiae* yeast systems(Arnesen et al., 2009a).

Based on our *in vitro* activity data, it is noteworthy that both human Naa10 and Naa50 catalytic subunits display lower K_m values for their respective peptide substrates and increased catalytic efficiencies, when they are in the NatA/Naa50 relative to when they are not in complex. Meanwhile, we observed that the other substrate, acetyl-CoA, while not showing detectable binding to *Sp*Naa50, binds to *Sp*NatA/Naa50 about 4.5-fold tighter than *Sp*NatA alone. It is likely that *Sp*Naa50 facilitates acetyl-CoA binding to *Sp*NatA and the structural observation that *Sc*Naa50 sits closely to the Q/RxxGxG/A acetyl-CoA binding motif of *Sc*Naa10 provides a plausible explanation for how *Sp*Naa50 may modulate the acetyl-CoA binding activity of *Sp*NatA. Taken together, we conclude that in human, NatA and Naa50 have cooperative effects on their acetylation activities when associating together, while in yeast, the inactive Naa50 still contributes to NatA activity, which is consistent with previous result that reduction of some NatA type N-termini was detected in yeast Naa50 deletion mutants (Van Damme et al., 2015) We note that the cooperative effects between NatA and Naa50 that we observed *in vitro* are based only on single cognate NatA and Naa50 peptide substrates. It

is currently unknown if the degree of cooperation varies with different peptide substrates.

One surprising aspect of the *Sc*NatA/Naa50 structure is the identification of Inositol hexaphosphate (IP_6), which bridges interactions between the Naa10 and Naa15 subunits of NatA with a dissociation constant in the sub-mircomolar range. A similar role for IP_6 was identified in the recently reported hNatA/HYPK complex (Gottlieb and Marmorstein, 2018), suggesting an evolutionarily conserved role of IP_6 in stabilizing the NatA complex. Since IP_6 has long been appreciated to have many signaling properties in diverse organisms including yeast and mammals (Abul Kalam and Sanchita, 2012), it is also possible that IP_6 may have a yet unidentified signaling role in NatA function.

HYPK is an important regulatory protein that binds to hNatA but is not conserved in *S. pombe* or *S. cerevisiae*. Recent structural studies suggest that HYPK was a nanomolar dissociation constant NatA binding partner and that HYPK binding likely inhibits Naa50 binding (Weyer et al., 2017, Gottlieb and Marmorstein, 2018). Here we have demonstrated that hNaa50 can promote hNatA acetylation activity. We propose that the slightly divergent association mechanism between NatA and Naa50 in yeast and human may be related to the presence of HYPK in human and higher eukaryotes but not in most yeast. It will be of interest to further investigate the interplay among these binding partners within the tetrameric human NatA/Naa50/HYPK complex.

We find in our study that *Sp*Naa50 is catalytically inactive, and this is likely due to its reduced affinity for acetyl-CoA and the relative narrowness of the peptide substrate binding site of *Sc*Naa50 observed in the *Sc*NatA/Naa50 structure. Surprisingly, we observed binding between *Sc*Naa50 and acetyl-

CoA, although the optimal acetyl-CoA binding motif is missing in both *Sc*Naa50 and *Sp*Naa50. Nonetheless, both *Sc*Naa50 and *Sp*Naa50 are catalytically inactive in out acetyltransferase assays. We propose that the yeast lineage lost catalytically active Naa50 at least due to the lack of peptide substrate binding. Indeed, unlike metazoans, *Sc*Naa50 knock out displays no phenotype (Gautschi et al., 2003). In another study, no impact on Met-starting yeast N-termini was observed where yeast Naa50 was deleted (Van Damme et al., 2015). Meanwhile, Naa50 has functional roles in sister chromatic cohesion in higher organism, independent of the NatA complex, which is not observed in yeast (Rong et al., 2016, Ribeiro et al., 2016, Williams et al., 2003). Thus, yeast Naa50 is very likely enzymatically inactive, only providing extra stability and regulatory roles for NatA, including participation in ribosome binding (see below). We propose that Naa50 substrates are processed by NatC, which recognizes a similar cognate sequence.

A recent cryo-EM structure of a native *Sc*NatA/Naa50-ribosome structure, where the ribosome is resolved to 3.4 Å and the NatA/Naa50 portion is resolved to about 8 Å resolution, indicates that NatA/Naa50 associates with the ribosome through interaction with the ribosomal RNA expansion segments involving predominantly Naa15, but also Naa50 (Knorr et al., 2018). While Naa10 is positioned proximal to the ribosome peptide exit tunnel, Naa50 is remote from the peptide exit tunnel. A docking of our 2.7 Å resolution NatE structure onto the cryo-EM structure (PDB: 6HD7) provides a pseudo-3.4 Å resolution structure of the NatE-ribosome complex (**Figure 8**). This superposition reveals that Naa50 is positioned ~80 Å away from the peptide exit tunnel of the ribosome, consistent with the finding of Knorr et al. that approximates this distance to be ~ 85 Å (Knorr et al., 2018). As this observation suggests that peptides emerging from the ribosome exit tunnel encounter the Naa10 active site prior to the Naa50 active site, we speculate that it is likely that Naa50 requires a longer nascent chain for acetylation.

However, we found that *Sp*Naa50 binding slightly promotes *Sp*NatA acetylation catalytic efficiency. This effect could be more significant in the context of the ribosome, given that Knorr et al. observe that Naa50 makes contact to the ribosome RNA expansion segment, thus also playing a role in NatA recruitment to the ribosome. Such a contribution to NatA-ribosome recruitment by Naa50 is consistent with a recent observation that *D. melanogaster* Naa50 knockout impairs NatA acetylation activity *in vivo* (Rathore et al., 2016). We placed the Naa10 acetyl CoA binding site by overlapping our structure to the *Sp*NatA structure in complex with bi-substrate analogue (PDB:4KVM) and found that the acetyl-CoA binding sites for both Naa10 and Naa50 are oriented in the same direction and facing the ribosome nascent peptide exit tunnel and separated by a distance of only 26.6 Å (**Figure 8**). It is likely that the relative position of these two catalytic subunits, Naa10 and Naa50, might change on the ribosome to accommodate the cognate peptide substrate that emerges out of the ribosome exit tunnel. We propose that the flexibility of the hNatA-Naa50 interface (as suggested by the relatively high B-factor of Naa50 relative to NatA) may also facilitate movement of Naa50 closer to the ribosome exit tunnel once its cognate substrate is in proximity for N-terminal acetylation. This might be facilitated further if human Naa50 did not participate in NatA anchoring to the ribosome as it does in the yeast system. Additional interactions might be compensated through the binding of HYPK.

Taken together, our biochemical and structural characterization of ternary NatA/Naa50 complexes in yeast and human in this study has provided new and significant insights into the association and regulatory mechanism of this unusual dual enzyme system. These studies set the stage for future studies to decipher the molecular mechanism of the human NatA/Naa50/HYPK complex. In addition, our identification of mutants that prevent NatA/Naa50

association in yeast and humans will facilitate analysis of the uncoupling of co- and post-translational protein acetylation by Naa50.

ACKNOWLEDGMENTS

This work was supported by NSF grant CHE-1708759 to E.J.P. and NIH grant R35 GM118090 awarded to R.M. We acknowledge the support of the Perelman School of Medicine, University of Pennsylvania DNA Sequencing Core Facility and E. Dean from the High Throughput Screening Core Facility for providing the Sf9 cells containing human NatA/Naa50 for this study. We thank Adam Olia as well as Dan Ricketts for helpful discussions.

AUTHOR CONTRIBUTIONS

Conceptualization, S.D., R.S.M. and R.M.; Methodology, S.D., R.S.M, and R.M.; Investigation, S.D., X.W., B.P.; Formal Analysis, S.D., X.W. and B.P.; Writing – Original Draft, S.D.; Visualization, S.D.; Writing – Review and Editing, S.D., R.S.M., X.W., B.P., E.J.P. and R.M.; Funding Acquisition; R.M.; Resources, R.M.; Supervision, R.M. and E.J.P..

DECLARATION OF INTERESTS

The authors declare no competing interest.

MAIN FIGURE TITILES AND LEGENDS

Table 1. Data Statistics for *Sc*NatA/Naa50 Crystal structure

Table 2. Catalytic Parameters for NatA, Naa50, and NatA/Naa50 against peptide substrate

Figure 1. NatA and Naa50 form stable complexes in yeast and human.

(A) Gel filtration elution profiles of Naa50 with NatA in *S. pombe* (top),human (middle), and cross-species between yeast *S. pombe* and *S. cerevisiae* (bottom), using a Superdex S200 column, with either 200 mM or 1M NaCl in sizing buffer. Coomassie-stained SDS–PAGE of peak fractions are shown to the right of the chromatograms.

(B) Fluorescence polarization assays with NatA titrated into fluorescein-5-maleimide labeled Naa50 in both *S. pombe* (left) and human (right) systems. The data is fit to calculate a dissociation constant between NatA and Naa50.

(C) Differential scanning fluorimetry assays of NatA alone or with Naa50 in both *yeast* and human systems. Recorded melting temperature transitions are indicated.

Figure 2. Crystal structure of the ternary NatA/Naa50 complex shows that Naa50 contacts both subunits of NatA.

(A) *Sc*Naa10 (yellow), *Sc*Naa15(cyan), and *Sc*Naa50 (violet) are shown in cartoon. The N-terminal two alpha helices (residues 1-53) of Naa15 are not resolved and not shown in the structure. Several alpha helices of Naa15 that contribute to Naa10 and Naa50 binding are labeled.

(B) Zoom-in view of the interface between Naa50, Naa10 and Naa15. Residues that contribute to interactions between Naa10 and Naa50 are shown.

(C) Zoom-in view showing key residues involved in interactions with IP6.

(D) Representative isothermal titration calorimetry (ITC) of curve of IP6 titrated into *Sp*NatA with the calculated dissociation constant indicated.

Figure 3. Hydrophobic interactions dominate the ScNatA-ScNaa50 binding interface.

(A) Zoom-in view of the major hydrophobic binding interface between Naa15 and Naa50 with residues that participate in interaction shown.

(B) Zoom-in view of the contacts between Naa10 and Naa50 with residues that participate in interaction shown.

Figure 4. The NatA/Naa50 complex promotes catalytic crosstalk.

(A) Time course acetylation activity of *Sp*Naa50, *Sp*NatA/Naa50, hNaa50, hNatA/Naa50, *Sc*Naa50 and *Sc*NatA/Naa50 against the MLGP peptide substrate.

(B) Michaelis–Menten kinetic curve of hNaa50 and hNatA/Naa50 against the MLGP peptide substrate.

(C) Michaelis–Menten kinetic curve of hNatA and hNatA/Naa50 against the SASE peptide substrate.

(D) Michaelis–Menten kinetic curve of SpNatA and SpNatA/Naa50 against the SASE peptide substrate.

Figure 5. Weak acetyl-CoA binding activity and a narrow substrate binding grove contributes to the catalytic inactivity of yeast Naa50.

(A) Representative ITC curve of acetyl-CoA titrated into hNaa50.

(B) Representative ITC curve of acetyl-CoA titrated into *Sp*Naa50.

(C) Representative ITC curve of acetyl-CoA titrated into SpNatA. The calculated dissociation constant is indicated.

(D) Representative ITC curve of acetyl-CoA titrated into SpNatA/Naa50. The calculated dissociation constant is indicated.

(E) Representative ITC curve of acetyl-CoA titrated into GST-*Sc*Naa50.

(F) Representative ITC curve of acetyl-CoA titrated into GST-*Sp*Naa50.

(G) Representative ITC curve of acetyl-CoA titrated into free GST.

(H) Superimposition of *Sc*Naa50 and hNaa50 (PDB: 3TFY) structures.

Figure 6. NatA TY mutants are unable to pull-down Naa50 and co-migrate with Naa50.

(A) GST pull-down assay with NatA/Naa50 mutants to interrogate the contribution of residues in Naa50-NatA association.

(B) Gel filtration elution profiles of Naa50 with either wild-type (dotted red line taken from Figure 1A) or TY mutants (blue line) of NatA using a Superdex S200 column. Coomassie-stained SDS–PAGE of peak fractions of Naa50 with NatA TY mutants shown below the chromatograms.

Figure 7. NatA TY mutants disrupt NatA/Naa50 complex interactions.

(A) Fluorescence polarization assays of NatA TY mutants and Naa50 in *S. pombe* and human.

(B) Differential scanning fluorimetry assays of NatA TY mutants with and without Naa50. Recorded melting temperature transitions are indicated.

(C) Comparison of acetylation activity of NatA wild-type and TY mutants. Activities are normalized to WT protein activity level.

Figure 8. Docking of our ScNatA/Naa50 crystal structure onto the ribosome-NatA/Naa50 Cryo-EM structure. The *Sc*NatA/Naa50 crystal structure is aligned to the NatA/Naa50-ribosome structure (PDB: 6HD7). The magnified view shows that Naa10 is most proximal to the ribosome peptide exit tunnel, while the acetyl-CoA binding sites of Naa10 and Naa50 are facing the same side.

STAR Methods text

CONTACT FOR REAGENT AND RESOURCE SHARING

Further information and requests for resources and reagents should be directed to and will be fulfilled by the Lead Contact, Ronen Marmorstein (marmor@upenn.edu).

EXPERIMENTAL MODEL

We used *E.coli* Rosetta (DE3)pLysS cells for recombinant expression of *Sc*NatA/Naa50, *Sp*NatA, *Sp*Naa50, and hNaa50 for biochemical and biophysical experiments. The cells were cultured using standard practices in LB media.

We used *Spodoptera frugiperda* (Sf9) cells cultured in SFM II medium for the recombinant expression of hNatA for biochemical, biophysical, and X-ray crystallography experiments.

METHOD DETAILS

NatA and Naa50 expression and purification

Human NatA(hNatA), human Naa50(hNaa50), and *Schizosaccharomyces pombe* NatA(SpNatA) were expressed and purified as described previously(Liszczak et al., 2013, 2018, Liszczak et al., 2011). Full-length *Schizosaccharomyces pombe* Naa50(spNaa50) was cloned into pRSF with a N-terminal GST fusion, and expressed and purified with the same method as described for spNatA(Liszczak et al., 2013). Full-length *Saccharomyces cerevisiae* Naa15(ScNaa15) was cloned into pRSF_Duet vector with a N terminal PolyHis tag and a Tobacco Etch Virus (TEV) cleavage site. C-terminal truncated ScNaa10(1-226) with no tag was cloned into pET_Duet, and un-tagged full-length *Sc*Naa50 was cloned into pCDF-Duet. To express the ternary *Sc*Naa10-*Sc*Naa15-*Sc*Naa50 complex (*Sc*NatA/Naa50 complex), these three plasmids were co-transformed into Rosetta (DE3)pLysS competent *E. coli* cells, which were grown to an OD_{600} of 1 and induced with

0.5 mM of Isopropyl β-D-1-thiogalactopyranoside (IPTG) at 16 °C for ~16 h. ScNatA/Naa50 complex purification procedure was modified from SpNatA as described (Liszczak et al., 2013). Cells were isolated by centrifugation for 20 mins at 4500 rpm and lysed by sonication in a buffer containing 25 mM Tris, pH 8.0, 500 mM NaCl, 0.1 mg/mL PMSF. After centrifugation, the supernatant was isolated and passed over Ni-resin (Thermo Scientific), which was subsequently washed with 10 column volumes of lysis buffer supplemented with 25 mM imidazole and 10 mM 2-mercaptoethanol. Protein was eluted with 300 mM imidazole and dialyzed into buffer containing 25 mM sodium citrate monobasic, pH 5.5, 10 mM NaCl and 10 mM 2-mercaptoethanol. Protein was purified with a 5-mL HiTrap SP ion-exchange column and eluted in a salt gradient (10–700 mM NaCl). Peak fractions were concentrated to ~ 0.5 mL with a 100-kDa concentrator (Amicon Ultra, Millipore), and loaded onto an S200 gel-filtration column (GE Healthcare) in a buffer containing 25 mM HEPES, pH 7.0, 200 mM NaCl, 5% glycerol and 1 mM TCEP. Proteins were aliquoted, snap-frozen in liquid nitrogen, and stored at −80 °C for further use. Full-length *Sc*Naa50 was cloned into pRSF with a N-terminal GST tag and a TEV cleavage site, to express and purify *Sc*Naa50 alone. We observed that *Sc*Naa50 was not stable in the absence of the GST tag and absorbs minimally at 280 nm. We therefore only worked with GST-*Sc*Naa50 in biochemical experiments. GST-*Sc*Naa50 was purified using the same method as described above. Concentrations of hNatA, hNaa50, *Sp*NatA, *Sp*Naa50, *Sc*NatA/Naa50 and GST-*Sc*Naa50 were determined by absorbance at 280 nm and using their extinction coefficient of 132,480 $cm^{-1}M^{-1}$,13,410 $cm^{-1}M^{-1}$, 120,000 $cm^{-1}M^{-1}$, 14,440 $cm^{-1}M^{-1}$, 151,800 $cm^{-1}M^{-1}$, and 58,790 $cm^{-1}M^{-1}$, respectively. All protein mutants were generated using the QuikChange protocol from Stratagene and obtained following the expression and purification protocols described above.

Fluorescence polarization (FP) assays

There are five cysteine residues present in *Sp*Naa50 (Cys22, Cys54, Cys60, and Cys96) and four cysteine residues in hNaa50 (Cys60, Cys61, Cys79, and Cys100). We found that we did not have to make mutations to obtain the fluorescein labeled Naa50, which suggested that at least one cysteine in each is exposed to solvent. 25-fold excess of Fluorescein-5-Maleimide (ThermoFisher) was added into about 100 µL of 1 mg/ml purified hNaa50 or *Sp*Naa50 in sizing buffer. The reaction was quenched with 2-mercaptoethanol after overnight incubation at 4°C. Excess Fluorescein-5-Maleimide was removed by S75 gel-filtration chromatography. To run the assays,10 nM of labeled Naa50 was used in all reactions, and NatA concentrations were varied to determine the dissociation constant (K_d). 5 mg/mL BSA and 0.2% v/v Tween were added into the reaction buffer (25 mM HEPES, pH 7.0, 200 mM NaCl and 10 mM DTT) to prevent non-specific binding. FP readings were recorded with a Perkin Elmer EnVision and each curve was repeated in triplicate. GraphPad Prism, version 5.01, was used for all data fitting. Errors were reported in Standard Deviation (SD) with $n = 3$.

Acetyltransferase activity assays

All the acetyltransferase assays were performed essentially as previously described (Liszczak et al., 2013, Liszczak et al., 2011) and carried out at room temperature in the reaction buffer containing 75 mM HEPES, pH 7.0, 120 mM NaCl, 1 mM DTT. The SASE substrate peptide (NH_2-SASEAGVRWGRPVGRRRRP-COOH; GenScript) and the MLGP substrate peptide (NH_2-MLGPEGGRWGRPVGRRRRP-COOH; GenScript) were used to determine the enzymatic activity of NatA and Naa50, respectively. For measuring Naa50 activity, a time course of activity was carried out with either 500 nM of SpNaa50, SpNatA/SpNaa50, hNaa50, hNatA/hNaa50, ScNaa50, and ScNatA/Naa50 mixed with 300 µM of C^{14} labeled acetyl-CoA (4 mCi $mmol^{-1}$; PerkinElmer Life Sciences), and 500 µM MLGP peptide in a 100 µL reaction volume. To quench the reaction at specific times, 15 µL of the

reaction mixture was added to P81 paper discs (Whatman), and the paper discs were immediately placed in wash buffer with 10 mM HEPES, pH 7.5. Unreacted acetyl-CoA is removed by washing at least three times. Paper discs were dried with acetone and mixed with 4 mL scintillation fluid for signal measurement by a Packard Tri-Carb 1500 liquid scintillation analyzer. Data was plotted with GraphPad Prism, version 5.01. To determine steady-state catalytic parameters, enzymes were mixed with 500 μM C^{14} labeled acetyl-CoA and the corresponding peptide substrate concentration was varied. A 20 μL reaction were performed but only 15 μL of the reaction mixture was quenched onto the paper discs after specific times. For assaying hNaa50 and hNatA/hNaa50 against MLGP peptide, 300 nM enzyme was used in 40-minute reactions. For assaying hNatA and hNatA/hNaa50 against SASE peptide, 100 nM enzyme was used in 12-minute reactions. For assaying SpNatA and SpNatA/SpNaa50 against SASE peptide, 50 nM enzyme was used in 10-minute reactions. Paper disc washes and signal reading steps were performed in the same manner as mentioned above. GraphPad Prism, version 5.01, was used for all kinetic data fitting to the Michaelis–Menten equation. Each curve was repeated at least 3 times. For NatA TY mutant activity tests, 100 nM of SpNatA, SpNatA-T412Y, hNatA, and hNatA-T406Y were mixed with 300 μM of C^{14} labeled acetyl-CoA and 500 μM of peptide substrate for 30-minutes reactions. Signals were normalized to the WT activity, and errors were reported in Standard Error of the Mean (SEM) with $n = 3$.

Size exclusion chromatography assays

A total of 500 μl of purified NatA (4.2 μM) and purified Naa50 (12.6 μM) was injected onto a S200 gel-filtration column (GE Healthcare). UV absorbance values were normalized to the maximum value of the first elution peak, then plotted against the elution volume in GraphPad Prism, version 5.01. Only elution volumes around the NatA, Naa50 and NatA/Naa50 elution peaks are

shown in the figures. Corresponding peak fractions were run on SDS-PAGE and stained with colloidal Coomassie blue for imaging.

GST pull-down assays

1 μM of GST tagged Naa50 and 5 μM of NatA was incubate with 50 μL of glutathione agarose resin at 4 °C for 1 hour in reaction buffer containing 25 mM HEPES, pH 7.0, 200 mM NaCl and 1 mM TCEP. Resin was then washed extensively with the same buffer and eluted with glutathione. Samples were collected for analysis on SDS-PAGE.

Differential scanning fluorimetry assays

Sypro Orange (5000X stock, ThermoFisher Scientific) was diluted 1:200 and 4 μL was mixed with 16 μL solution with 5 μM NatA and 5 μM Naa50 in sizing buffer. Fluorescent readings were recorded using a qPCR (ABI 7900 RealTime PCR) with a 2% ramp rate, while heated from 20 °C to 95 °C. Melting curves were generated from these readings and melting temperatures were determined by taking the first derivative of the curves. DSF scans of all samples were performed in triplicate. Error bars in the figure indicated the Standard Deviation (SD) of each sample.

ITC measurements

Measurements were recorded on a MicroCal iTC200 at 20 °C. Samples were dialyzed into buffer containing 25 mM HEPES pH 7.0, 200 mM NaCl, 1 mM DTT. Protein samples (*Sp*Naa50, *Sp*NatA, *Sp*NatA/Naa50, GST-SpNaa50, GST-ScNaa50, and GST) with concentrations of 50 μM in the cell and 1mM of acetyl-CoA in the syringe were used in the experiments. For hNaa50, 100 μM protein and 0.5 mM of acetyl-CoA was used. The raw data was analyzed with MicroCal ITC analysis software.

***Sc*NatA/Naa50 crystallization and data collection**

Ternary *Sc*NatA/Naa50 complex was mixed with 3 molar excess of NatA bisubstrate inhibitor (CoA-SASEA), Naa50 bisubstrate inhibitor (CoA-MLGPE) and IP6. Bisubstrate inhibitors were prepared as previously described (Liszczak et al., 2013). Crystals were grown within ~3 days by hanging drop vapor diffusion at 20 °C at 7.5 mg/ml, using one to one drop ratios against reservoir solution containing 10% PEG 3350, 0.1 M Sodium Malonate (pH 5.0). Crystals were transferred into mother liquor supplemented with 25% glycerol and flash-frozen in liquid nitrogen. Data were collected at the Advanced Photon Source (beamline 24-ID-C) and processed using HKL2000 (Otwinowski and Minor, 1997).

_Sc_NatA/Naa50 structure determination and refinement

The collected diffraction data showed strong anisotropy and ellipsoidal truncation and anisotropic scaling was performed (Strong et al., 2006). The resolution limit along a*, b*, c* are 2.7 Å, 3.4 Å, 2.7 Å, respectively. The crystal structure of ScNatA/Naa50 was determined by molecular replacement using a structure of unpublished ScNatE (PDB ID Code: 4XNH) without ligand or solvent molecules as a search model. Molecular replacement was done using Phaser in Phenix(Adams et al., 2010). Initial Manual model building was done in Coot (Emsley and Cowtan, 2004) and all subsequent rounds of refinement were performed using Phenix refine and Coot interchangeably. Refinement statistics can be found in **Table 1**. The final model and structure factors were submitted to the Protein Data Bank with code 6O07 (Research Collaboratory for Structural Bioinformatics).

Distance calculations, as well as three-dimensional alignment r.m.s. deviations and graphics were generated in PyMOL (http:// www.pymol.org/)

Sequence alignments in the manuscript were performed using Clustal Omega (https://www.ebi.ac.uk/Tools/msa/clustalo/) and visualized using ESPript 3.0(Robert and Gouet, 2014) (http://espript.ibcp.fr/ESPript/ESPript/)

All surface area calculations were performed using PDBePISA (Proteins, Interfaces, Structures and Assemblies) (http://www.ebi.ac.uk/pdbe/pisa/)

QUANTIFICATION AND STATISTICAL ANALYSIS

In fluorescence polarization assays, K_d errors in the figure were generated by GraphPad Prism with a one-site binding model with n = 3 and value errors were reported as SD.

In acetyltransferase activity assays, kinetic curve error bars were generated by GraphPad Prism with Michaelis–Menten equation fitting, with n = 3. In WT and TY mutant activities comparison test, error bars in the figure were reported as SEM with n = 3.

In differential scanning fluorimetry assays, error bars in melting temperatures were indicated as SD with n = 3.

In ITC measurements, K_d errors were generated by MicroCal ITC software with a single-site binding mode fitting analysis.

DATA AND SOFTWARE AVAILABILITY

Coordinates of the structure described in this article have been deposited in the PDB with accession numbers PDB: 6O07

REFERENCES

ABUL KALAM, S. & SANCHITA, B. 2012. IP6 (Inositol Hexaphosphate) as a Signaling Molecule. *Current Signal Transduction Therapy,* 7**,** 289-304.

ADAMS, P. D., AFONINE, P. V., BUNKOCZI, G., CHEN, V. B., DAVIS, I. W., ECHOLS, N., HEADD, J. J., HUNG, L.-W., KAPRAL, G. J., GROSSE-KUNSTLEVE, R. W., MCCOY, A. J., MORIARTY, N. W., OEFFNER, R., READ, R. J., RICHARDSON, D. C., RICHARDSON, J. S., TERWILLIGER, T. C. & ZWART, P. H. 2010. PHENIX: a comprehensive Python-based system

for macromolecular structure solution. *Acta Crystallographica Section D,* 66**,** 213-221.

AKSNES, H., DRAZIC, A., MARIE, M. & ARNESEN, T. 2016. First Things First: Vital Protein Marks by N-Terminal Acetyltransferases. *Trends in Biochemical Sciences,* 41**,** 746-760.

AKSNES, H., GORIS, M., STROMLAND, O., DRAZIC, A., WAHEED, Q., REUTER, N. & ARNESEN, T. 2017. Molecular determinants of the N-terminal acetyltransferase Naa60 anchoring to the Golgi membrane. *J Biol Chem,* 292**,** 6821-6837.

AKSNES, H., VAN DAMME, P., GORIS, M., STARHEIM, K. K., MARIE, M., STOVE, S. I., HOEL, C., KALVIK, T. V., HOLE, K., GLOMNES, N., FURNES, C., LJOSTVEIT, S., ZIEGLER, M., NIERE, M., GEVAERT, K. & ARNESEN, T. 2015. An organellar nalpha-acetyltransferase, naa60, acetylates cytosolic N termini of transmembrane proteins and maintains Golgi integrity. *Cell Rep,* 10**,** 1362-74.

AMETZAZURRA, A., LARREA, E., CIVEIRA, M. P., PRIETO, J. & ALDABE, R. 2008. Implication of human N-alpha-acetyltransferase 5 in cellular proliferation and carcinogenesis. *Oncogene,* 27**,** 7296-306.

ARNESEN, T., ANDERSON, D., BALDERSHEIM, C., LANOTTE, M., VARHAUG, J. E. & LILLEHAUG, J. R. 2005. Identification and characterization of the human ARD1-NATH protein acetyltransferase complex. *Biochem J,* 386**,** 433-43.

ARNESEN, T., GROMYKO, D., PENDINO, F., RYNINGEN, A., VARHAUG, J. E. & LILLEHAUG, J. R. 2006a. Induction of apoptosis in human cells by RNAi-mediated knockdown of hARD1 and NATH, components of the protein N-alpha-acetyltransferase complex. *Oncogene,* 25**,** 4350-60.

ARNESEN, T., GROMYKO, D., PENDINO, F., RYNINGEN, A., VARHAUG, J. E. & LILLEHAUG, J. R. 2006b. Induction of apoptosis in human cells by RNAi-mediated knockdown of hARD1 and NATH, components of the protein N-α-acetyltransferase complex. *Oncogene,* 25**,** 4350.

ARNESEN, T., STARHEIM, K. K., VAN DAMME, P., EVJENTH, R., DINH, H., BETTS, M. J., RYNINGEN, A., VANDEKERCKHOVE, J., GEVAERT, K. & ANDERSON, D. 2010. The chaperone-like protein HYPK acts together with NatA in cotranslational N-terminal acetylation and prevention of Huntingtin aggregation. *Mol Cell Biol,* 30**,** 1898-909.

ARNESEN, T., VAN DAMME, P., POLEVODA, B., HELSENS, K., EVJENTH, R., COLAERT, N., VARHAUG, J. E., VANDEKERCKHOVE, J., LILLEHAUG, J. R., SHERMAN, F. & GEVAERT, K. 2009a. Proteomics analyses reveal the evolutionary conservation and divergence of N-terminal acetyltransferases from yeast and humans. *Proceedings of the National Academy of Sciences,* 106**,** 8157.

ARNESEN, T., VAN DAMME, P., POLEVODA, B., HELSENS, K., EVJENTH, R., COLAERT, N., VARHAUG, J. E., VANDEKERCKHOVE, J., LILLEHAUG, J. R., SHERMAN, F. & GEVAERT, K. 2009b. Proteomics analyses reveal the evolutionary conservation and divergence of N-terminal acetyltransferases

from yeast and humans. *Proceedings of the National Academy of Sciences,* 106**,** 8157-8162.

BEHNIA, R., PANIC, B., WHYTE, J. R. C. & MUNRO, S. 2004. Targeting of the Arf-like GTPase Arl3p to the Golgi requires N-terminal acetylation and the membrane protein Sys1p. *Nature Cell Biology,* 6**,** 405.

CHU, C. W., HOU, F., ZHANG, J., PHU, L., LOKTEV, A. V., KIRKPATRICK, D. S., JACKSON, P. K., ZHAO, Y. & ZOU, H. 2011. A novel acetylation of beta-tubulin by San modulates microtubule polymerization via down-regulating tubulin incorporation. *Mol Biol Cell,* 22**,** 448-56.

DIKIY, I. & ELIEZER, D. 2014. N-terminal Acetylation Stabilizes N-terminal Helicity in Lipid- and Micelle-bound α-Synuclein and Increases Its Affinity for Physiological Membranes. *Journal of Biological Chemistry,* 289**,** 3652-3665.

DINH, T. V., BIENVENUT, W. V., LINSTER, E., FELDMAN-SALIT, A., JUNG, V. A., MEINNEL, T., HELL, R., GIGLIONE, C. & WIRTZ, M. 2015. Molecular identification and functional characterization of the first Nalpha-acetyltransferase in plastids by global acetylome profiling. *Proteomics,* 15**,** 2426-35.

DORFEL, M. J. & LYON, G. J. 2015. The biological functions of Naa10-From amino-terminal acetylation to human disease. *Gene,* 567**,** 103-131.

DRAZIC, A., AKSNES, H., MARIE, M., BOCZKOWSKA, M., VARLAND, S., TIMMERMAN, E., FOYN, H., GLOMNES, N., REBOWSKI, G., IMPENS, F., GEVAERT, K., DOMINGUEZ, R. & ARNESEN, T. 2018. NAA80 is actin's N-terminal acetyltransferase and regulates cytoskeleton assembly and cell motility. *Proc Natl Acad Sci U S A*.

EMSLEY, P. & COWTAN, K. 2004. Coot: model-building tools for molecular graphics. *Acta Crystallographica Section D,* 60**,** 2126-2132.

EVJENTH, R., HOLE, K., KARLSEN, O. A., ZIEGLER, M., ARNESEN, T. & LILLEHAUG, J. R. 2009. Human Naa50p (Nat5/San) displays both protein N alpha- and N epsilon-acetyltransferase activity. *J Biol Chem,* 284**,** 31122-9.

FLUGE, Ø., BRULAND, O., AKSLEN, L. A., VARHAUG, J. E. & LILLEHAUG, J. R. 2002. NATH, a novel gene overexpressed in papillary thyroid carcinomas. *Oncogene,* 21**,** 5056-5068.

GAUTSCHI, M., JUST, S., MUN, A., ROSS, S., RüCKNAGEL, P., DUBAQUIé, Y., EHRENHOFER-MURRAY, A. & ROSPERT, S. 2003. The Yeast Nα-Acetyltransferase NatA Is Quantitatively Anchored to the Ribosome and Interacts with Nascent Polypeptides. *Molecular and Cellular Biology,* 23**,** 7403-7414.

GIGLIONE, C., FIEULAINE, S. & MEINNEL, T. 2015. N-terminal protein modifications: Bringing back into play the ribosome. *Biochimie,* 114**,** 134-146.

GORIS, M., MAGIN, R. S., FOYN, H., MYKLEBUST, L. M., VARLAND, S., REE, R., DRAZIC, A., BHAMBRA, P., STøVE, S. I., BAUMANN, M., HAUG, B. E., MARMORSTEIN, R. & ARNESEN, T. 2018. Structural determinants and cellular environment define processed actin as the sole substrate of the N-

terminal acetyltransferase NAA80. *Proceedings of the National Academy of Sciences*.

GOTTLIEB, L. & MARMORSTEIN, R. 2018. Structure of Human NatA and Its Regulation by the Huntingtin Interacting Protein HYPK. *Structure,* 26**,** 925-935.e8.

HOLMES, W. M., MANNAKEE, B. K., GUTENKUNST, R. N. & SERIO, T. R. 2014. Loss of amino-terminal acetylation suppresses a prion phenotype by modulating global protein folding. *Nature Communications,* 5**,** 4383.

HONG, H. Y., CAI, Y. F., ZHANG, S. J., DING, H. Y., WANG, H. T. & HAN, A. D. 2017. Molecular Basis of Substrate Specific Acetylation by N-Terminal Acetyltransferase NatB. *Structure,* 25**,** 641-+.

HOU, F., CHU, C.-W., KONG, X., YOKOMORI, K. & ZOU, H. 2007. The acetyltransferase activity of San stabilizes the mitotic cohesin at the centromeres in a shugoshin-independent manner. *The Journal of Cell Biology,* 177**,** 587-597.

HUA, K. T., TAN, C. T., JOHANSSON, G., LEE, J. M., YANG, P. W., LU, H. Y., CHEN, C. K., SU, J. L., CHEN, P. B., WU, Y. L., CHI, C. C., KAO, H. J., SHIH, H. J., CHEN, M. W., CHIEN, M. H., CHEN, P. S., LEE, W. J., CHENG, T. Y., ROSENBERGER, G., CHAI, C. Y., YANG, C. J., HUANG, M. S., LAI, T. C., CHOU, T. Y., HSIAO, M. & KUO, M. L. 2011. N-alpha-acetyltransferase 10 protein suppresses cancer cell metastasis by binding PIX proteins and inhibiting Cdc42/Rac1 activity. *Cancer Cell,* 19**,** 218-31.

HWANG, C.-S., SHEMORRY, A. & VARSHAVSKY, A. 2010. N-Terminal Acetylation of Cellular Proteins Creates Specific Degradation Signals. *Science,* 327**,** 973-977.

JEONG, J. W., BAE, M. K., AHN, M. Y., KIM, S. H., SOHN, T. K., BAE, M. H., YOO, M. A., SONG, E. J., LEE, K. J. & KIM, K. W. 2002. Regulation and destabilization of HIF-1alpha by ARD1-mediated acetylation. *Cell,* 111**,** 709-20.

KALVIK, T. V. & ARNESEN, T. 2012. Protein N-terminal acetyltransferases in cancer. *Oncogene,* 32**,** 269.

KNORR, A. G., SCHMIDT, C., TESINA, P., BERNINGHAUSEN, O., BECKER, T., BEATRIX, B. & BECKMANN, R. 2018. Ribosome–NatA architecture reveals that rRNA expansion segments coordinate N-terminal acetylation. *Nature Structural & Molecular Biology*.

LEE, C. F., OU, D. S., LEE, S. B., CHANG, L. H., LIN, R. K., LI, Y. S., UPADHYAY, A. K., CHENG, X., WANG, Y. C., HSU, H. S., HSIAO, M., WU, C. W. & JUAN, L. J. 2010. hNaa10p contributes to tumorigenesis by facilitating DNMT1-mediated tumor suppressor gene silencing. *J Clin Invest,* 120**,** 2920-30.

LISZCZAK, G., ARNESEN, T. & MARMORSTEIN, R. 2011. Structure of a ternary Naa50p (NAT5/SAN) N-terminal acetyltransferase complex reveals the molecular basis for substrate-specific acetylation. *J Biol Chem,* 286**,** 37002-10.

LISZCZAK, G., GOLDBERG, J. M., FOYN, H., PETERSSON, E. J., ARNESEN, T. & MARMORSTEIN, R. 2013. Molecular basis for N-terminal acetylation by the heterodimeric NatA complex. *Nat Struct Mol Biol,* 20**,** 1098-105.

MAGIN, R. S., DENG, S., ZHANG, H., COOPERMAN, B. & MARMORSTEIN, R. 2017. Probing the interaction between NatA and the ribosome for co-translational protein acetylation. *PLOS ONE,* 12**,** e0186278.

MAGIN, R. S., LISZCZAK, G. P. & MARMORSTEIN, R. 2015. The Molecular Basis for Histone H4-and H2A-Specific Amino-Terminal Acetylation by NatD. *Structure,* 23**,** 332-341.

MYKLEBUST, L. M., STOVE, S. I. & ARNESEN, T. 2015. Naa10 in development and disease. *Oncotarget,* 6**,** 34041-2.

OTWINOWSKI, Z. & MINOR, W. 1997. Processing of X-ray diffraction data collected in oscillation mode. *Methods in Enzymology.* Academic Press.

PAVLOU, D. & KIRMIZIS, A. 2016. Depletion of histone N-terminal-acetyltransferase Naa40 induces p53-independent apoptosis in colorectal cancer cells via the mitochondrial pathway. *Apoptosis,* 21**,** 298-311.

POLEVODA, B., BROWN, S., CARDILLO, T. S., RIGBY, S. & SHERMAN, F. 2008. Yeast N-alpha-terminal acetyltransferases are associated with ribosomes. *Journal of Cellular Biochemistry,* 103**,** 492-508.

POLEVODA, B. & SHERMAN, F. 2003. Composition and function of the eukaryotic N-terminal acetyltransferase subunits. *Biochemical and Biophysical Research Communications,* 308**,** 1-11.

RATHORE, O. S., FAUSTINO, A., PRUDêNCIO, P., VAN DAMME, P., COX, C. J. & MARTINHO, R. G. 2016. Absence of N-terminal acetyltransferase diversification during evolution of eukaryotic organisms. *Scientific Reports,* 6**,** 21304.

RIBEIRO, A. L., SILVA, R. D., FOYN, H., TIAGO, M. N., RATHORE, O. S., ARNESEN, T. & MARTINHO, R. G. 2016. Naa50/San-dependent N-terminal acetylation of Scc1 is potentially important for sister chromatid cohesion. *Scientific Reports,* 6**,** 39118.

ROBERT, X. & GOUET, P. 2014. Deciphering key features in protein structures with the new ENDscript server. *Nucleic Acids Research,* 42**,** W320-W324.

RONG, Z., OUYANG, Z., MAGIN, R. S., MARMORSTEIN, R. & YU, H. 2016. Opposing Functions of the N-terminal Acetyltransferases Naa50 and NatA in Sister-chromatid Cohesion. *Journal of Biological Chemistry,* 291**,** 19079-19091.

ROPE, A. F., WANG, K., EVJENTH, R., XING, J., JOHNSTON, J. J., SWENSEN, J. J., JOHNSON, W. E., MOORE, B., HUFF, C. D., BIRD, L. M., CAREY, J. C., OPITZ, J. M., STEVENS, C. A., JIANG, T., SCHANK, C., FAIN, H. D., ROBISON, R., DALLEY, B., CHIN, S., SOUTH, S. T., PYSHER, T. J., JORDE, L. B., HAKONARSON, H., LILLEHAUG, J. R., BIESECKER, L. G., YANDELL, M., ARNESEN, T. & LYON, G. J. 2011. Using VAAST to identify an X-linked disorder resulting in lethality in male infants due to N-terminal acetyltransferase deficiency. *Am J Hum Genet,* 89**,** 28-43.

SCHIZA, V., MOLINA-SERRANO, D., KYRIAKOU, D., HADJIANTONIOU, A. & KIRMIZIS, A. 2013. N-alpha-terminal Acetylation of Histone H4 Regulates Arginine Methylation and Ribosomal DNA Silencing. *PLOS Genetics,* 9**,** e1003805.

SCOTT, D. C., MONDA, J. K., BENNETT, E. J., HARPER, J. W. & SCHULMAN, B. A. 2011. N-Terminal Acetylation Acts as an Avidity Enhancer Within an Interconnected Multiprotein Complex. *Science,* 334**,** 674-678.

SETTY, S. R. G., STROCHLIC, T. I., TONG, A. H. Y., BOONE, C. & BURD, C. G. 2004. Golgi targeting of ARF-like GTPase Arl3p requires its Nα-acetylation and the integral membrane protein Sys1p. *Nature Cell Biology,* 6**,** 414.

SHEMORRY, A., HWANG, C.-S. & VARSHAVSKY, A. Control of Protein Quality and Stoichiometries by N-Terminal Acetylation and the N-End Rule Pathway. *Molecular Cell,* 50**,** 540-551.

SONG, O. K., WANG, X., WATERBORG, J. H. & STERNGLANZ, R. 2003. An Nalpha-acetyltransferase responsible for acetylation of the N-terminal residues of histones H4 and H2A. *J Biol Chem,* 278**,** 38109-12.

STARHEIM, KRISTIAN K., ARNESEN, T., GROMYKO, D., RYNINGEN, A., VARHAUG, JAN E. & LILLEHAUG, JOHAN R. 2008. Identification of the human N^α-acetyltransferase complex B (hNatB): a complex important for cell-cycle progression. *Biochemical Journal,* 415**,** 325-331.

STARHEIM, K. K., GEVAERT, K. & ARNESEN, T. 2012. Protein N-terminal acetyltransferases: when the start matters. *Trends Biochem Sci,* 37**,** 152-61.

STARHEIM, K. K., GROMYKO, D., EVJENTH, R., RYNINGEN, A., VARHAUG, J. E., LILLEHAUG, J. R. & ARNESEN, T. 2009. Knockdown of human N alpha-terminal acetyltransferase complex C leads to p53-dependent apoptosis and aberrant human Arl8b localization. *Mol Cell Biol,* 29**,** 3569-81.

STOVE, S. I., MAGIN, R. S., FOYN, H., HAUG, B. E., MARMORSTEIN, R. & ARNESEN, T. 2016. Crystal Structure of the Golgi-Associated Human N alpha-Acetyltransferase 60 Reveals the Molecular Determinants for Substrate-Specific Acetylation. *Structure,* 24**,** 1044-1056.

STRONG, M., SAWAYA, M. R., WANG, S., PHILLIPS, M., CASCIO, D. & EISENBERG, D. 2006. Toward the structural genomics of complexes: crystal structure of a PE/PPE protein complex from Mycobacterium tuberculosis. *Proc Natl Acad Sci U S A,* 103**,** 8060-5.

TERCERO, J. C., DINMAN, J. D. & WICKNER, R. B. 1993. Yeast MAK3 N-acetyltransferase recognizes the N-terminal four amino acids of the major coat protein (gag) of the L-A double-stranded RNA virus. *Journal of bacteriology,* 175**,** 3192-3194.

VAN DAMME, P., EVJENTH, R., FOYN, H., DEMEYER, K., DE BOCK, P.-J., LILLEHAUG, J. R., VANDEKERCKHOVE, J., ARNESEN, T. & GEVAERT, K. 2011a. Proteome-derived Peptide Libraries Allow Detailed Analysis of the Substrate Specificities of Nα-acetyltransferases and Point to hNaa10p as the

Post-translational Actin Nα-acetyltransferase. *Molecular & Cellular Proteomics,* 10.

VAN DAMME, P., HOLE, K., GEVAERT, K. & ARNESEN, T. 2015. N-terminal acetylome analysis reveals the specificity of Naa50 (Nat5) and suggests a kinetic competition between N-terminal acetyltransferases and methionine aminopeptidases. *Proteomics,* 15**,** 2436-2446.

VAN DAMME, P., HOLE, K., PIMENTA-MARQUES, A., HELSENS, K., VANDEKERCKHOVE, J., MARTINHO, R. G., GEVAERT, K. & ARNESEN, T. 2011b. NatF contributes to an evolutionary shift in protein N-terminal acetylation and is important for normal chromosome segregation. *PLoS Genet,* 7**,** e1002169.

VAN DAMME, P., KALVIK, T. V., STARHEIM, K. K., JONCKHEERE, V., MYKLEBUST, L. M., MENSCHAERT, G., VARHAUG, J. E., GEVAERT, K. & ARNESEN, T. 2016. A Role for Human N-alpha Acetyltransferase 30 (Naa30) in Maintaining Mitochondrial Integrity. *Molecular & cellular proteomics : MCP,* 15**,** 3361-3372.

WEYER, F. A., GUMIERO, A., LAPOUGE, K., BANGE, G., KOPP, J. & SINNING, I. 2017. Structural basis of HypK regulating N-terminal acetylation by the NatA complex. *Nature communications,* 8**,** 15726-15726.

WILLIAMS, B. C., GARRETT-ENGELE, C. M., LI, Z., WILLIAMS, E. V., ROSENMAN, E. D. & GOLDBERG, M. L. 2003. Two putative acetyltransferases, san and deco, are required for establishing sister chromatid cohesion in Drosophila. *Curr Biol,* 13**,** 2025-36.

YANG, D., FANG, Q., WANG, M., REN, R., WANG, H., HE, M., SUN, Y., YANG, N. & XU, R.-M. 2013. Nα-acetylated Sir3 stabilizes the conformation of a nucleosome-binding loop in the BAH domain. *Nature Structural &Amp; Molecular Biology,* 20**,** 1116.

YI, C. H., SOGAH, D. K., BOYCE, M., DEGTEREV, A., CHRISTOFFERSON, D. E. & YUAN, J. 2007. A genome-wide RNAi screen reveals multiple regulators of caspase activation. *The Journal of cell biology,* 179**,** 619-626.

YOON, H., KIM, H. L., CHUN, Y. S., SHIN, D. H., LEE, K. H., SHIN, C. S., LEE, D. Y., KIM, H. H., LEE, Z. H., RYOO, H. M., LEE, M. N., OH, G. T. & PARK, J. W. 2014. NAA10 controls osteoblast differentiation and bone formation as a feedback regulator of Runx2. *Nat Commun,* 5**,** 5176.

YU, M., MA, M., HUANG, C., YANG, H., LAI, J., YAN, S., LI, L., XIANG, M. & TAN, D. 2009. Correlation of Expression of Human Arrest-Defective-1 (hARD1) Protein With Breast Cancer. *Cancer Investigation,* 27**,** 978-983.

Figure 1.

A

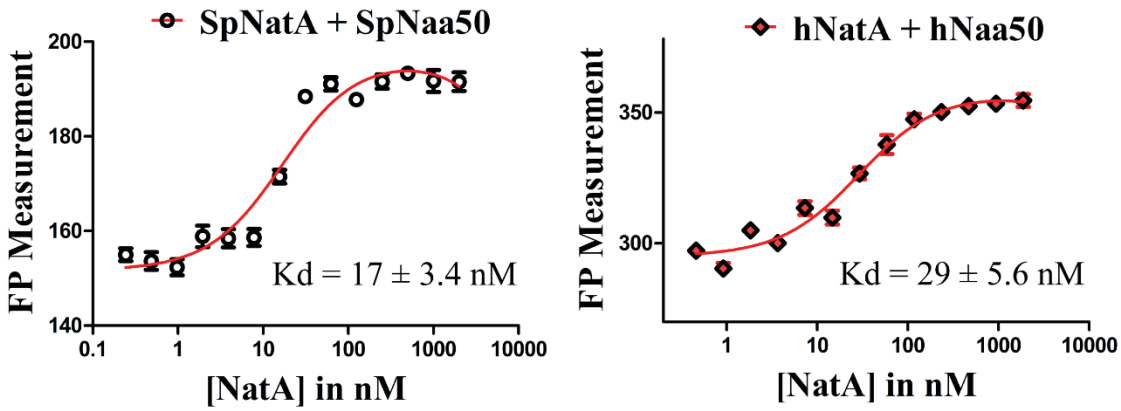
SpNatA + SpNaa50
FP Measurement
200
180
160
140
0.1
1
10
100
1000
10000
[NatA] in nM
Kd = 17 ± 3.4 nM
hNatA + hNaa50
FP Measurement
350
300
1
10
100
1000
10000
[NatA] in nM
Kd = 29 ± 5.6 nM

B

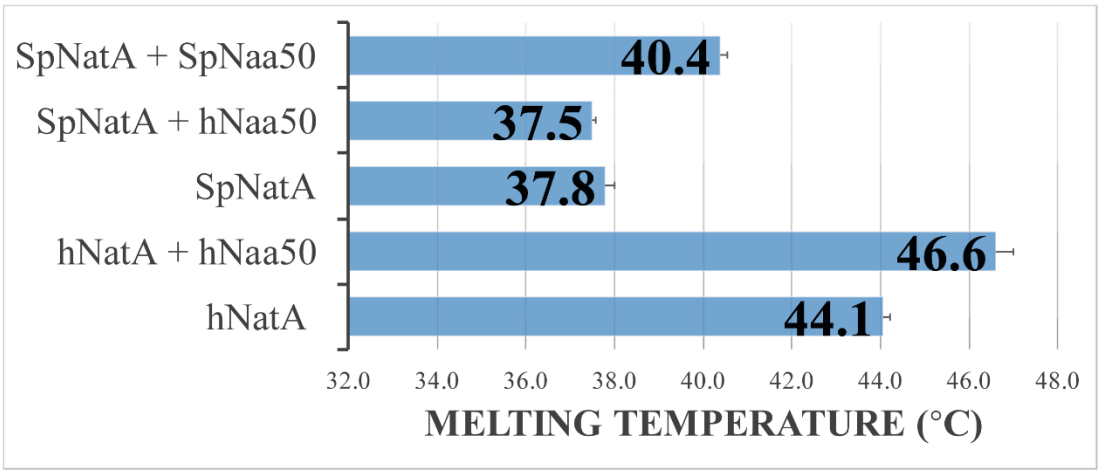
SpNatA + SpNaa50
40.4
SpNatA + hNaa50
37.5
SpNatA
37.8
hNatA + hNaa50
46.6
hNatA
44.1
32.0
34.0
36.0
38.0
40.0
42.0
44.0
46.0
48.0
MELTING TEMPERATURE (°C)

Figure 2.

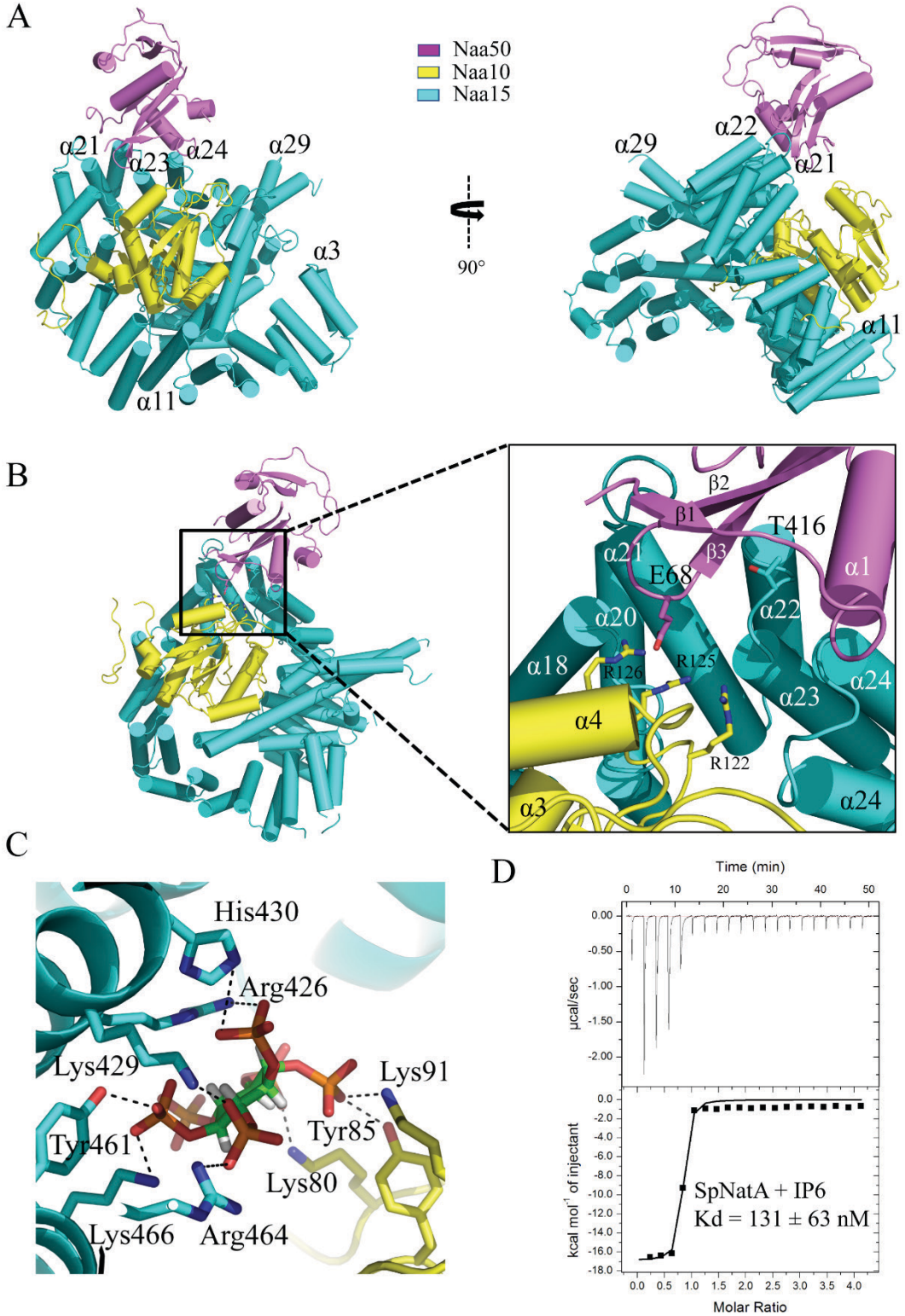
A
Naa50
Naa10
Naa15
α21
α23
α24
α29
α3
α11
90°
α29
α22
α21
α11
B
β2
β1
T416
α21
β3
E68
α1
α20
α22
α18
R126
R125
α24
α23
α4
R122
α3
α24
C
His430
Arg426
Lys429
Lys91
Tyr461
Tyr85
Lys80
Lys466
Arg464
D
Time (min)
0
10
20
30
40
50
0.00
-0.50
-1.00
-1.50
-2.00
µcal/sec
0.0
-2.0
-4.0
-6.0
-8.0
-10.0
-12.0
-14.0
-16.0
-18.0
kcal mol-1 of injectant
SpNatA + IP6
Kd = 131 ± 63 nM
0.0
0.5
1.0
1.5
2.0
2.5
3.0
3.5
4.0
Molar Ratio

Figure 3.

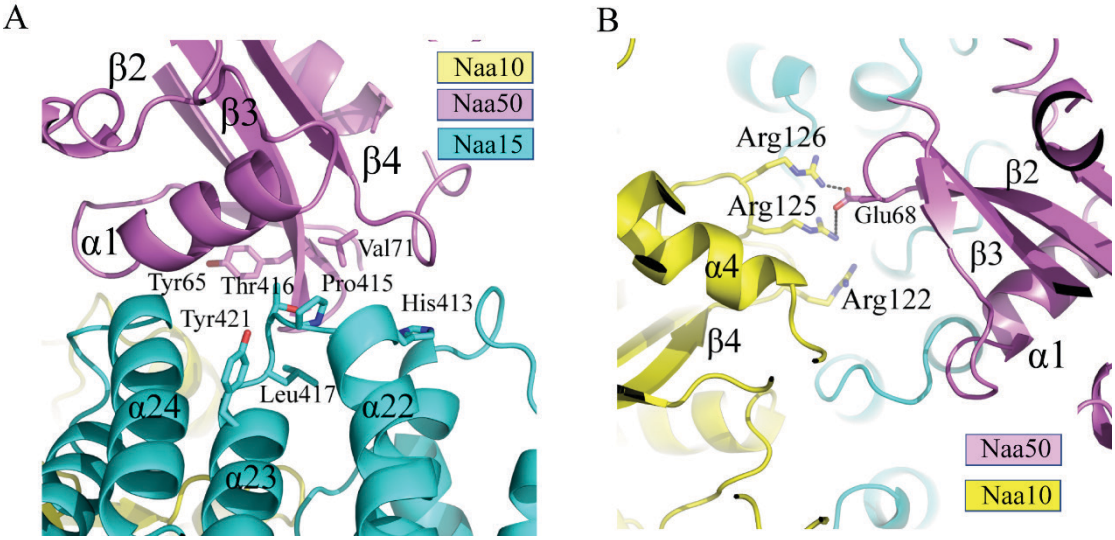
A
β2
β3
β4
α1
Naa10
Naa50
Naa15
Val71
Tyr65
Thr416
Pro415
His413
Tyr421
Leu417
α24
α22
α23
B
Arg126
Arg125
Glu68
β2
β3
α4
Arg122
β4
α1
Naa50
Naa10

Figure 4.

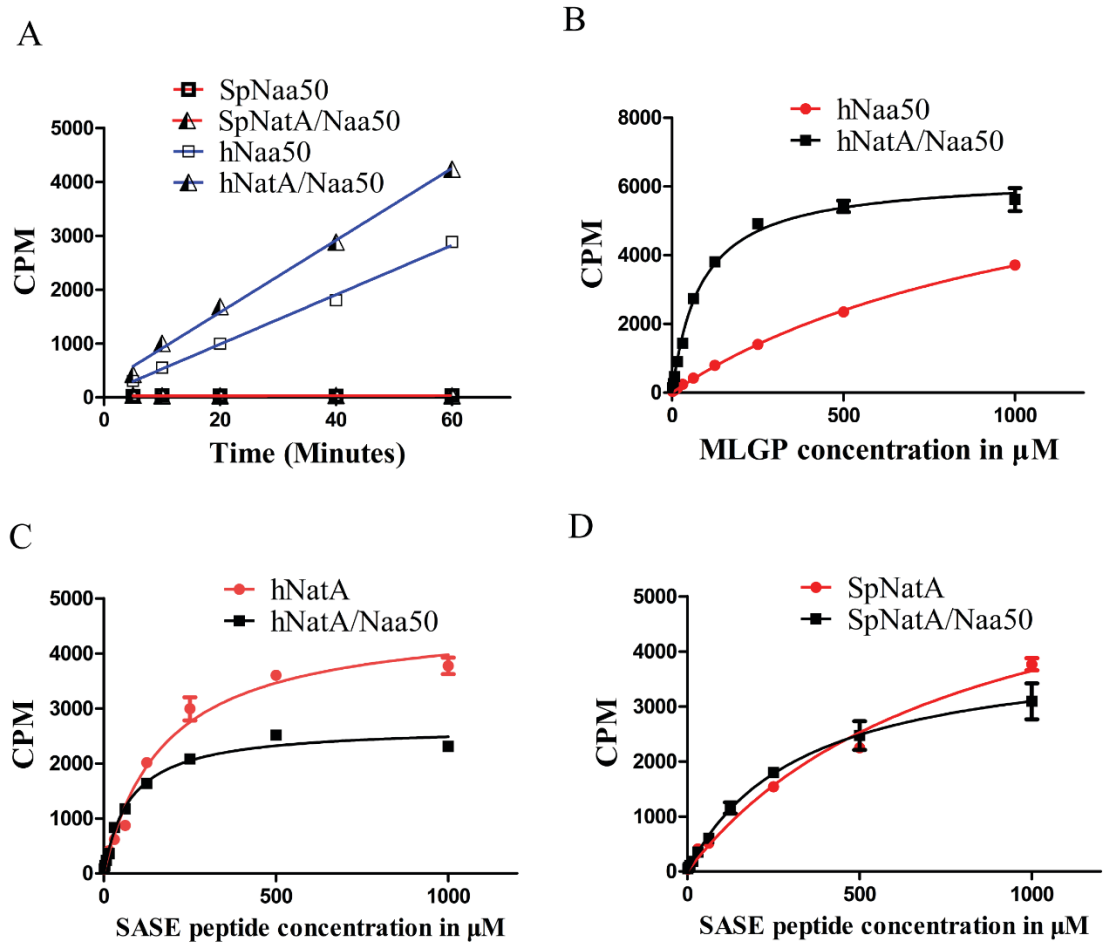
A
SpNaa50
SpNatA/Naa50
hNaa50
hNatA/Naa50
CPM
Time (Minutes)
B
hNaa50
hNatA/Naa50
CPM
MLGP concentration in µM
C
hNatA
hNatA/Naa50
CPM
SASE peptide concentration in µM
D
SpNatA
SpNatA/Naa50
CPM
SASE peptide concentration in µM

Figure 5.

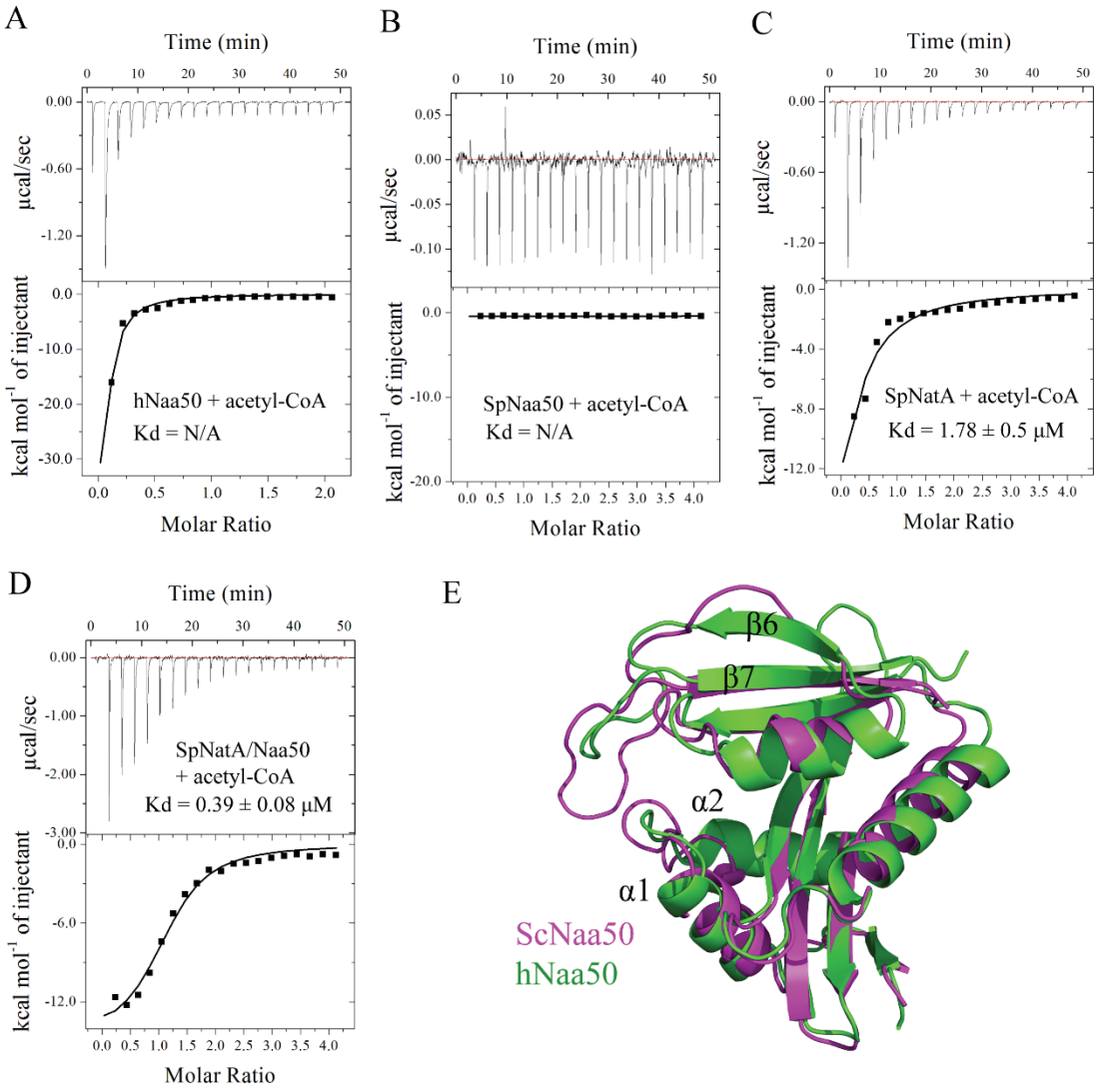
A
Time (min)
µcal/sec
kcal mol-1 of injectant
hNaa50 + acetyl-CoA
Kd = N/A
Molar Ratio
B
Time (min)
µcal/sec
kcal mol-1 of injectant
SpNaa50 + acetyl-CoA
Kd = N/A
Molar Ratio
C
Time (min)
µcal/sec
kcal mol-1 of injectant
SpNatA + acetyl-CoA
Kd = 1.78 ± 0.5 µM
Molar Ratio
D
Time (min)
µcal/sec
kcal mol-1 of injectant
SpNatA/Naa50
+ acetyl-CoA
Kd = 0.39 ± 0.08 µM
Molar Ratio
E
β6
β7
α2
α1
ScNaa50
hNaa50

Figure 6.

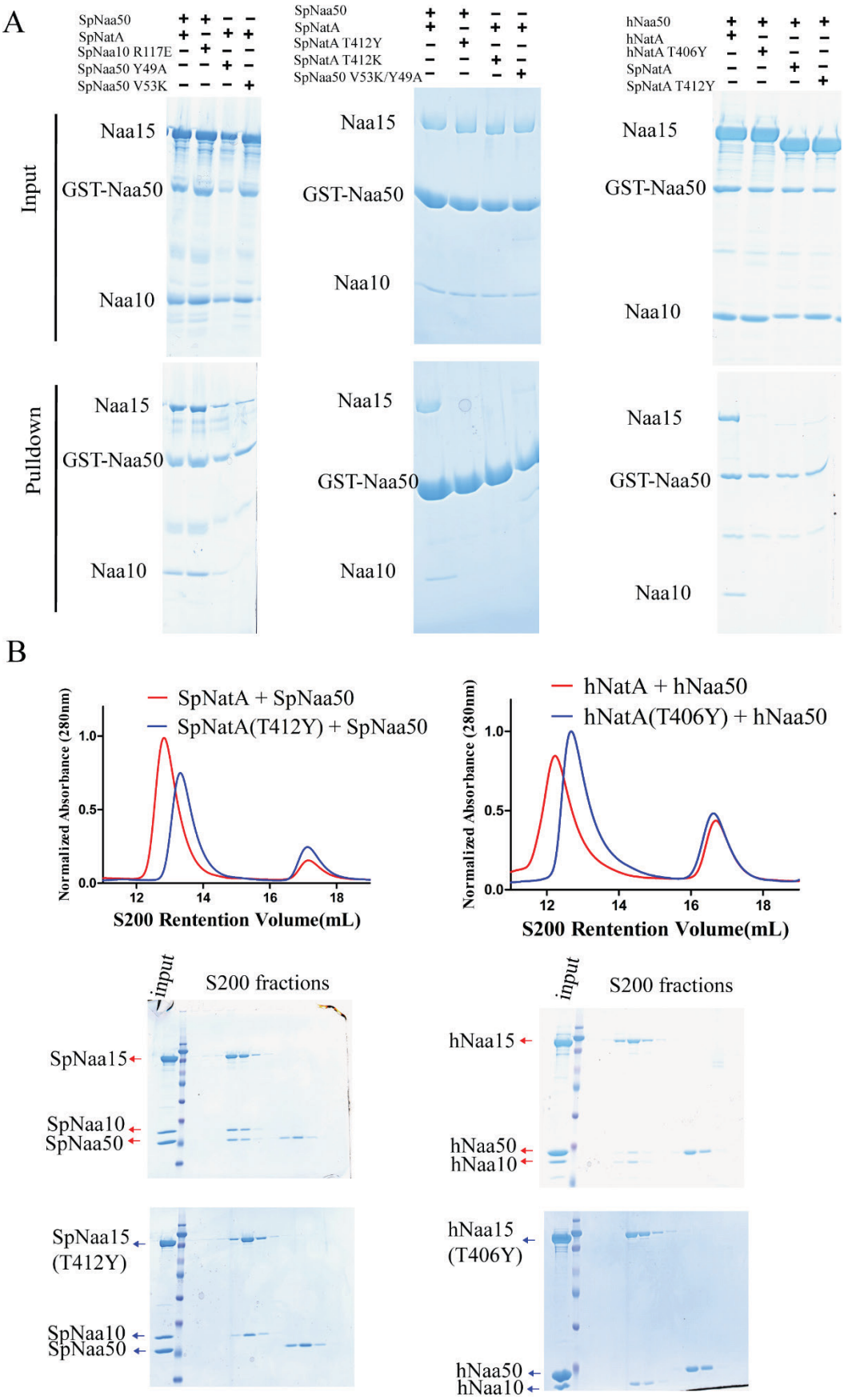
A
SpNaa50
SpNatA
SpNaa10 R117E
SpNaa50 Y49A
SpNaa50 V53K
SpNaa50
SpNatA
SpNatA T412Y
SpNatA T412K
SpNaa50 V53K/Y49A
hNaa50
hNatA
hNatA T406Y
SpNatA
SpNatA T412Y
Input
Pulldown
Naa15
GST-Naa50
Naa10
B
SpNatA + SpNaa50
SpNatA(T412Y) + SpNaa50
hNatA + hNaa50
hNatA(T406Y) + hNaa50
Normalized Absorbance (280nm)
S200 Rentention Volume(mL)
input
S200 fractions
SpNaa15
SpNaa10
SpNaa50
SpNaa15 (T412Y)
hNaa15
hNaa50
hNaa10
hNaa15 (T406Y)

Figure 7.

A

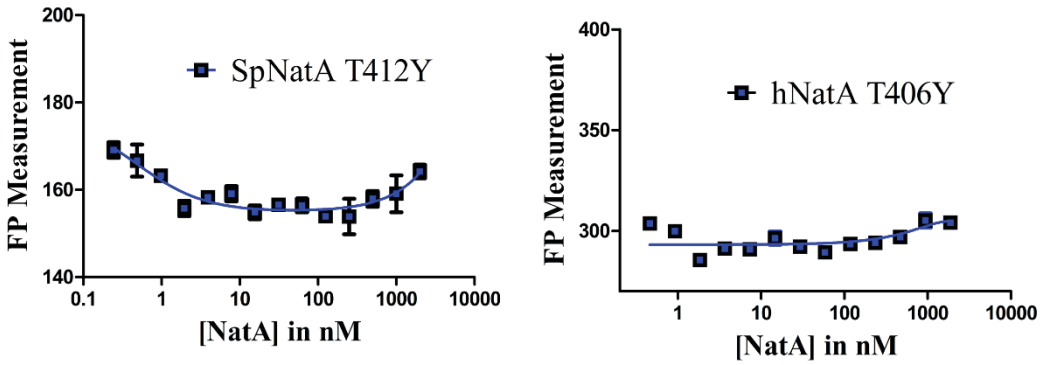
SpNatA T412Y
FP Measurement
200
180
160
140
0.1
1
10
100
1000
10000
[NatA] in nM
hNatA T406Y
FP Measurement
400
350
300
1
10
100
1000
10000
[NatA] in nM

B

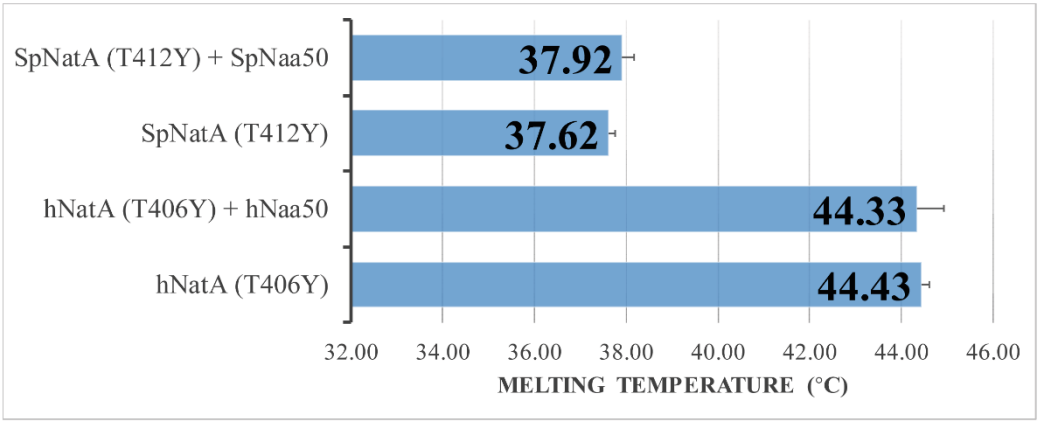
SpNatA (T412Y) + SpNaa50
37.92
SpNatA (T412Y)
37.62
hNatA (T406Y) + hNaa50
44.33
hNatA (T406Y)
44.43
32.00
34.00
36.00
38.00
40.00
42.00
44.00
46.00
MELTING TEMPERATURE (°C)

C

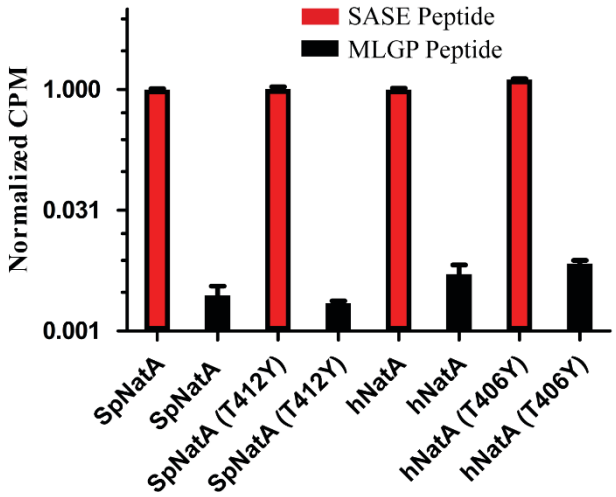
SASE Peptide
MLGP Peptide
Normalized CPM
1.000
0.031
0.001
SpNatA
SpNatA
SpNatA (T412Y)
SpNatA (T412Y)
hNatA
hNatA
hNatA (T406Y)
hNatA (T406Y)

Figure 8.

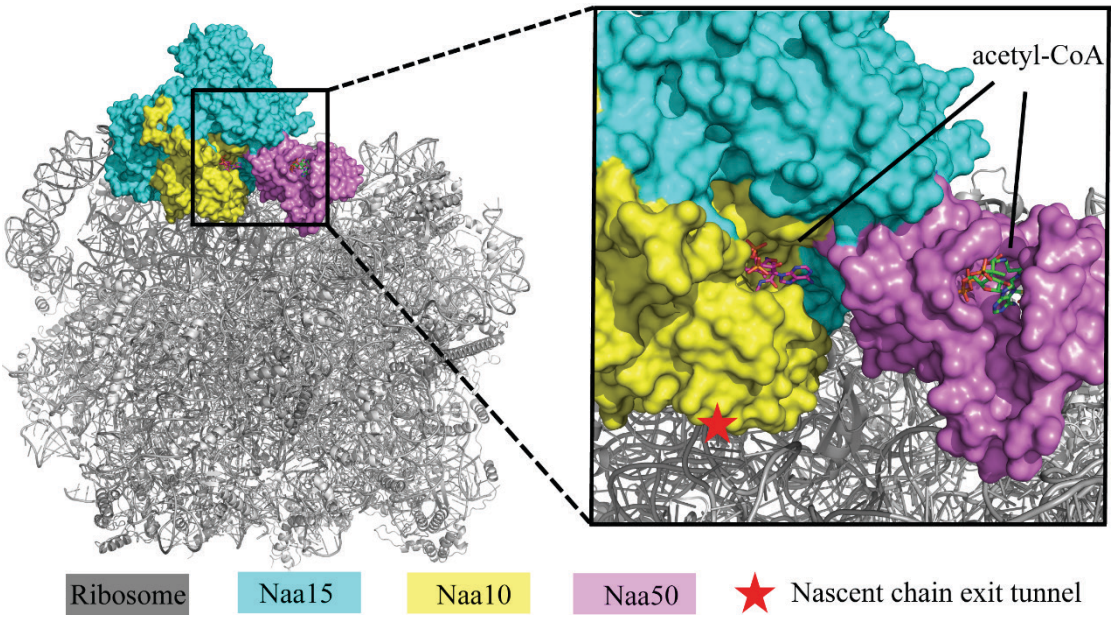
acetyl-CoA
Ribosome
Naa15
Naa10
Naa50
Nascent chain exit tunnel

TABLE 1, TABLE 2

Structure and mechanism of acetylation by the N-terminal dual enzyme NatA/Naa50 complex

Sunbin Deng, Robert S. Magin, Xuepeng Wei, Buyan Pan, E. James Petersson, Ronen Marmorstein

Table 1. Data Statistics for *Sc*NatA/Naa50 Crystal structure（PDB:6O07）

Crystal Parameters	
Space group	$P2_12_12_1$
Unit cell dimension	84.44(90)
a,b,c (Å)	125.73(90)
α, β, γ (°)	145.92(90)
Data collection	
Resolution (Å)	50 - 2.7 (3.0-2.7 *)
Unique reflections	41,731
R_{merge}	0.11 (0.18 *)
I/σ	13.11(1.923 *)
Completeness	99.3% (99.1% *)
Redundancy	6.1 (5.7 *)
Refinement	
R_{work}/R_{free}	0.2221/0.2503
Rmsd	
Bonds (Å)	0.002
Angels (°)	0.424
Average B factors (Å^2)	
Protein	58.26
Solvent	60.44
Ligand	83.58
Ramachandran statistics (%)	
Favored	94.3%
Allowed	5.7%
Outliers	0

*Values in parentheses are for highest-resolution shell.

Table 2. Catalytic Parameters for NatA, Naa50, and NatA/Naa50 against peptide substrate

	Normalized K_m	Normalized V_{max}	Normalized catalytic efficiency
SpNatA (SASE peptide)	1	1	1
SpNatA/Naa50 (SASE peptide)	0.41	0.63	1.54
hNatA (SASE peptide)	1	1	1
hNatA/Naa50 (SASE peptide)	0.43	0.57	1.33
hNaa50 (MLGP peptide)	1	1	1
hNatA/Naa50 (MLGP peptide)	0.071	0.77	10.8

Supplemental Information

Structure and mechanism of acetylation by the N-terminal dual enzyme NatA/Naa50 complex

Sunbin Deng, Robert S. Magin, Xuepeng Wei, Buyan Pan, E. James Petersson, Ronen Marmorstein

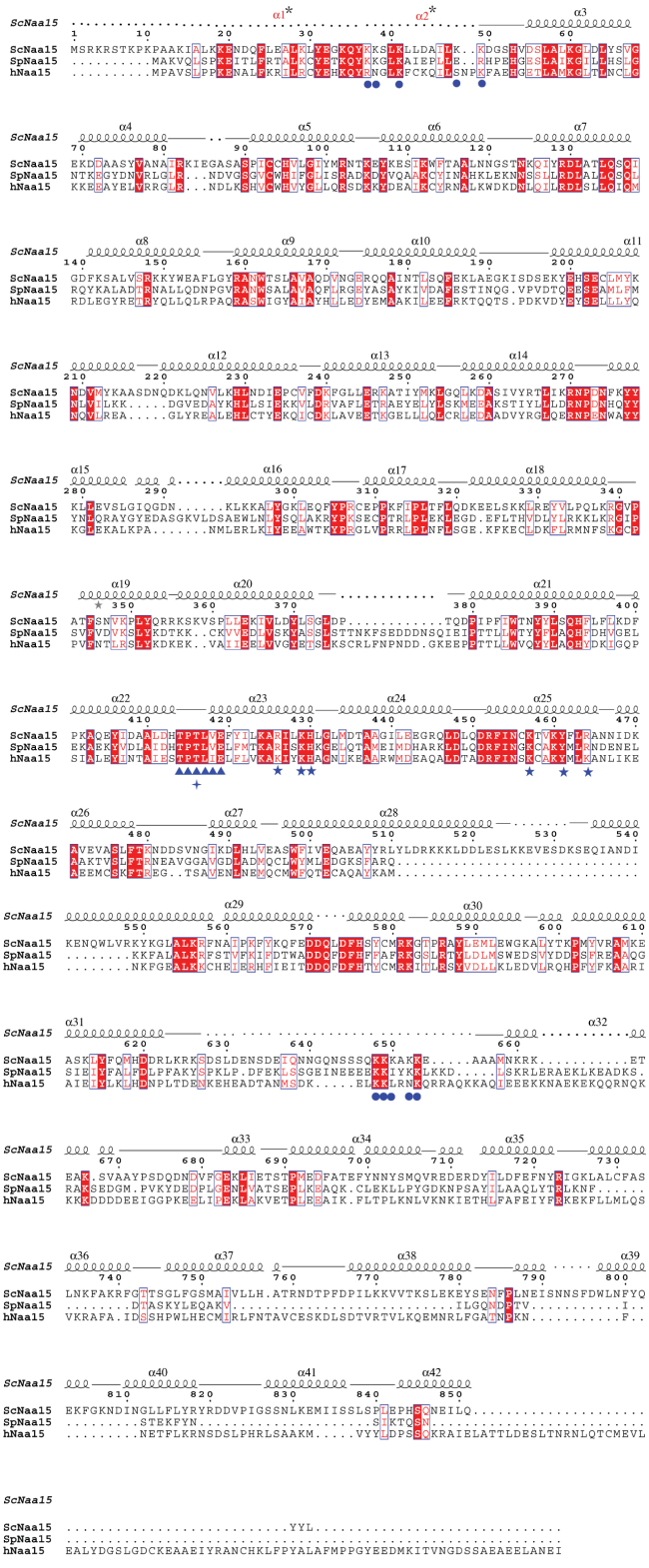

Figure S1. Related to Figure 2. Sequence alignment of Naa15 homologues from S. *cerevisiae* (Sc). S. pombe (Sp) and H. sapiens (h). ✦, threonine residue in TY mutants; ▲,TPTLXE motif for Naa50 binding; ★, residues binding IP6. ●, residues involving in ribsome association. The dotted lines indicates regions disordered and not resolved

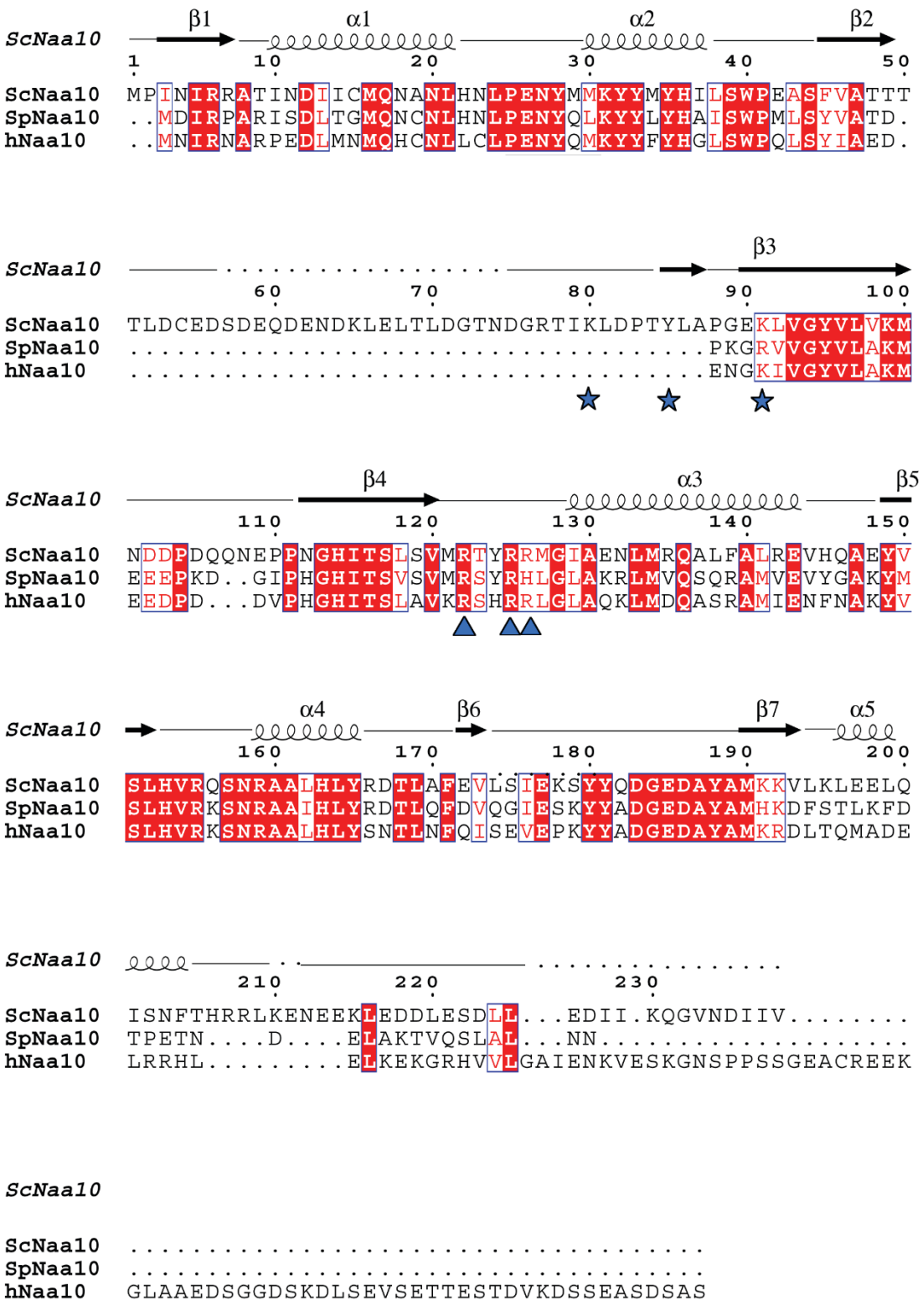

Figure S2. Related to Figure 2. Sequence alignment of Naa10 homologues from *S. cerevisiae* (Sc). S. pombe (Sp) and H. sapiens (h). ▲, residues contacting Naa50; ★, residues binding IP6.

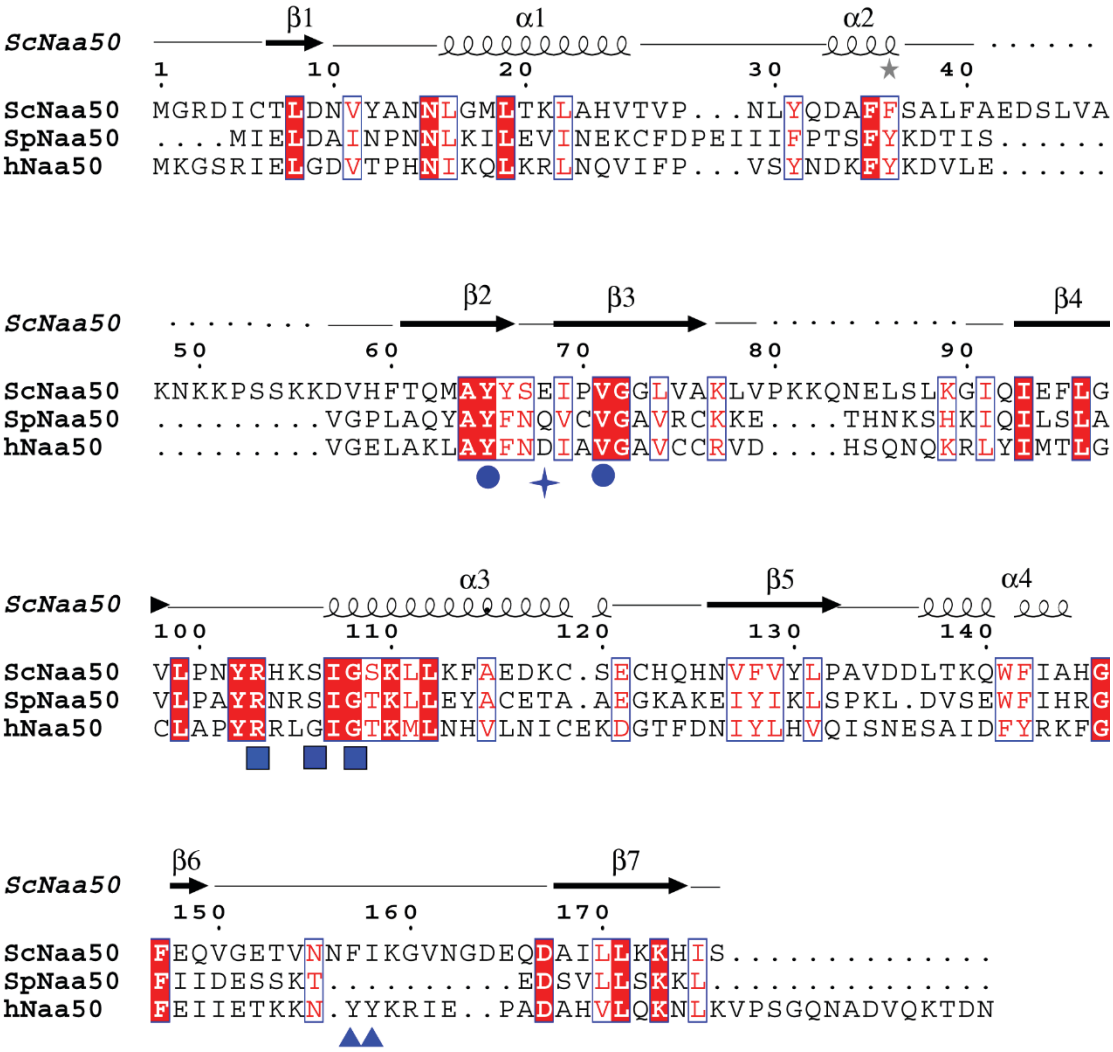

Figure S3. Related to Figure 2. Sequence alignment of Naa50 homologues from *S. cerevisiae* (Sc). S. pombe (Sp) and H. sapiens (h). ■, potential acetyl CoA binding motif; ● , residues involving NatA binding. ▲, YY motif in NATs for substrates binding

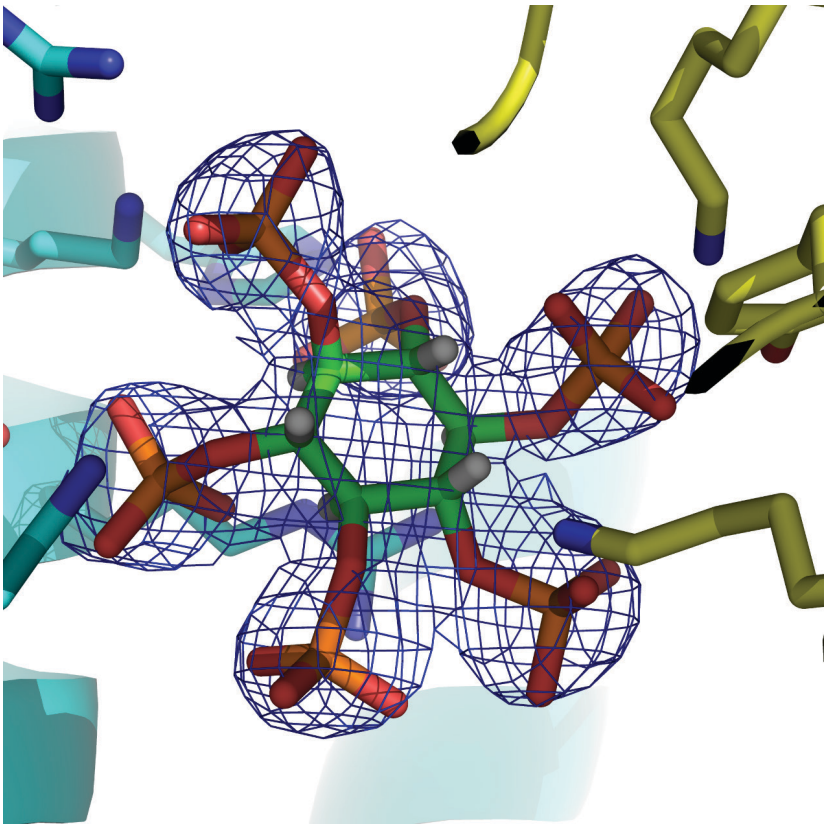

Figure S4. Related to Figure 2C. IP_6 2Fo-Fc electron density map of Naa50-bound to IP_6. The IP_6 electron density is contoured at 3.0 σ (shown in blue).